Geofluids (2005) **5**, 83–105

Hydrologic and geochemical controls on soluble benzene migration in sedimentary basins

Y. ZHANG, M. PERSON AND E. MERINO

Department of Geological Sciences, Indiana University, Bloomington, IN, USA

ABSTRACT

The effects of groundwater flow and biodegradation on the long-distance migration of petroleum-derived benzene in oil-bearing sedimentary basins are evaluated. Using an idealized basin representation, a coupled groundwater flow and heat transfer model computes the hydraulic head, stream function, and temperature in the basin. A coupled mass transport model simulates water washing of benzene from an oil reservoir and its miscible, advective/dispersive transport by groundwater. Benzene mass transfer at the oil–water contact is computed assuming equilibrium partitioning. A first-order rate constant is used to represent aqueous benzene biodegradation. A sensitivity study is used to evaluate the effect of the variation in aquifer/geochemical parameters and oil reservoir location on benzene transport. Our results indicate that in a basin with active hydrodynamics, miscible benzene transport is dominated by advection. Diffusion may dominate within the cap rock when its permeability is less than 10^{-19} m^2. Miscible benzene transport can form surface anomalies, sometimes adjacent to oil fields. Biodegradation controls the distance of transport down-gradient from a reservoir. We conclude that benzene detected in exploration wells may indicate an oil reservoir that lies hydraulically up-gradient. Geochemical sampling of hydrocarbons from springs and exploration wells can be useful only when the oil reservoir is located within about 20 km. Benzene soil gas anomalies may form due to regional hydrodynamics rather than separate phase migration. Diffusion alone cannot explain the elevated benzene concentration observed in carrier beds several km away from oil fields.

Key words: benzene, biodegradation, hydrodynamics, waterwashing

Received 24 February 2004; accepted 11 October 2004

Corresponding author: Ye Zhang, Department of Geological Sciences, Indiana University, 1001 East 10th Street, Bloomington, IN 47405-1405, USA.
Email: ylzhang@indiana.edu, Tel: 812-856-0139, Fax: 812-855-7899.

Geofluids (2005) **5**, 83–105

INTRODUCTION

Light aromatic hydrocarbons such as benzene, toluene, ethylbenzene and xylene (BTEX) are present in virtually every type of crude oil. They are also soluble in water and their aqueous solubilities increase with increasing temperature and pressure (IUPAC Solubility Data Series 1989). Field measurements of BTEX concentration can range from a few hundred ppm to 2000 ppm in crude oils and up to 18.6 ppm in oil field formation waters (Zarrella *et al.* 1967; Weisenburg *et al.* 1981). Benzene dissolved in formation water in contact with oil deposits is also observed to diminish at lateral distances on the order of 10 km (Table 1). BTEX sampled from exploration wells are thus used as indicators of undiscovered oil fields (Hunt 1979; Jones 1984; Burtell & Jones 1996). To estimate the distance to an unknown field, diffusion has been assumed as the primary transport mechanism (Fig. 1). Moreover, BTEX soil gas anomalies in the vicinity of oil fields have generated interest in using these compounds in surface geochemical exploration (Calhoun & Hawkins 1998, 1999). These anomalies have been attributed to vertical migration of (separate phase) BTEX gases from subsurface reservoirs (Calhoun & Hawkins 1998; Hawkins & Calhoun 2001). However, BTEX have boiling curves that do not intersect with the typical geothermal gradients of sedimentary basins (Aljoe *et al.* 1986; Helgeson *et al.* 1998; Fig. 2). And as components of liquid-phase petroleum, no evidence suggests that BTEX exist as an immiscible phase, e.g. either liquid or gas. On the contrary, in many oil-bearing basins, active groundwater flow systems can play an important role in the transport, formation and degradation of hydrocarbons (e.g. Hubbert 1953; Bredehoeft & Bennett 1971; Philp & Crisp 1982; Allin 1990; Tóth 1996). In particular,

Table 1 Benzene concentrations measured from formation waters located at different lateral distances from known oil fields, within equivalent zones of production (after Table 7, Zarrella *et al.* 1967).

Location	Geological formation	Benzene concentration in water (ppm)	Distance to production (miles)
New Mexico	Pennsylvanian	10.7	0.0
		6.5	2.0
Saskatchewan, Canada	Frobisher-Aldia	7.0	0.0
		4.5	1.0
		3.4	0.75
		2.2	1.75
		1.6	1.5
		1.0	5.5
Alberta, Canada	Leduc	4.8–6.0	0.0
		3.4	0.5
		2.2	1.5
		1.8	2.75
		1.6	2.75
West Texas	Wolfcamp	2.5	0.0
		1.2	0.75
		1.3	2.5
		0.9	5.0
		0.0	16.0

BTEX can dissolve into the regional groundwater and be subject to advective transport (Fig. 3). As the water table is neared, dissolved BTEX can volatize to form soil gases due to their high vapor pressure and low molecular weight (Schwille 1981). Benzene and toluene soil gas anomalies have been observed in groundwater discharge areas in east-central Alberta, but not directly over any known oil fields (Holysh & Tóth 1996). To date, miscible, advective transport of BTEX subsequent to reservoir charging has not been evaluated in the context of subsurface/surface geochemical prospecting.

BTEX dissolved in groundwater attenuate naturally in the subsurface. Attenuation processes include biodegradation, retardation, abiogenic reactions, and volatilization at the water table (Barker *et al.* 1987). In shallow groundwater flow systems and soils, biodegradation is considered the most important sink for BTEX. Numerous environmental studies have documented the consumption of BTEX by both aerobic and anaerobic bacteria (e.g. Jamison *et al.* 1976; Patrick & Barker 1985; Barker *et al.* 1987, 1989; Gillham and Burris, 1992; Barbaro *et al.* 1992; Allen-King *et al.* 1994; O'Leary *et al.* 1995; Weiner & Lovley 1998a,b; Burland & Edwards 1999; Schirmer *et al.* 1999). The rate of biodegradation is often rapid. In one study, benzene, toluene and xylene are found to attenuate within months in a shallow phreatic aquifer (Barker *et al.* 1989; Fig. 4). In this case, the attenuation of these compounds is attributed to aerobic biodegradation. Moreover, crude oil

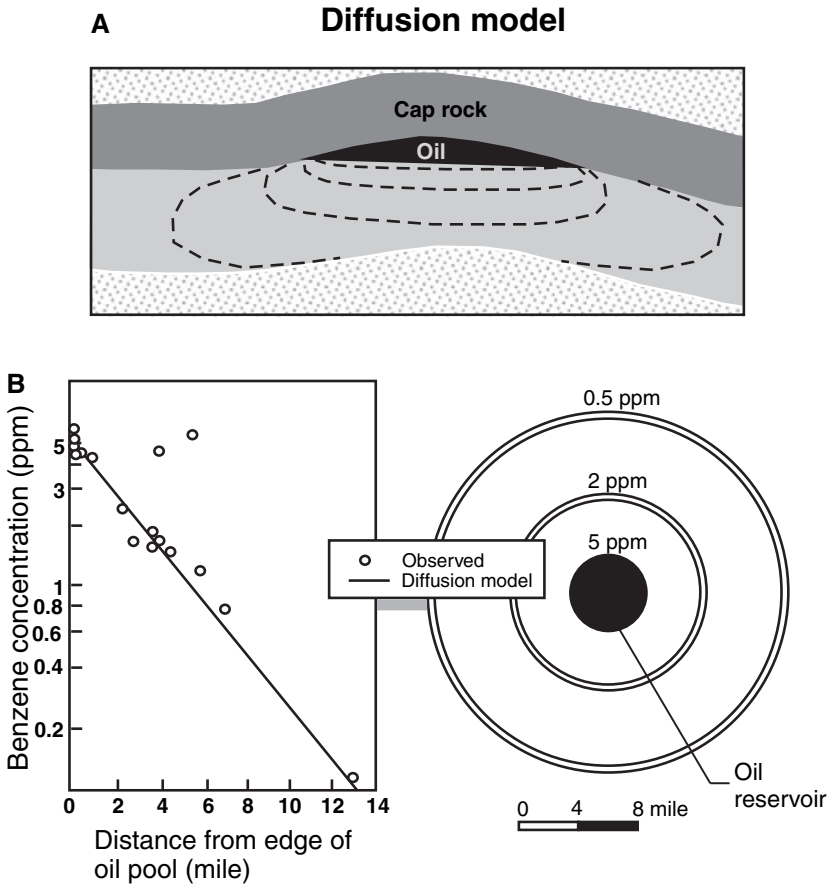

Fig. 1. (A) A cross-sectional schematic diagram representing transient, diffusive benzene transport within a carrier bed underlying an oil pool. (B) Log benzene concentrations (circles) versus distance from the edge of an oil pool in Nisku formation brine, Alberta (after Burtell & Jones 1996). The modeled concentration (line) is from a diffusion model (Burtell & Jones 1996).

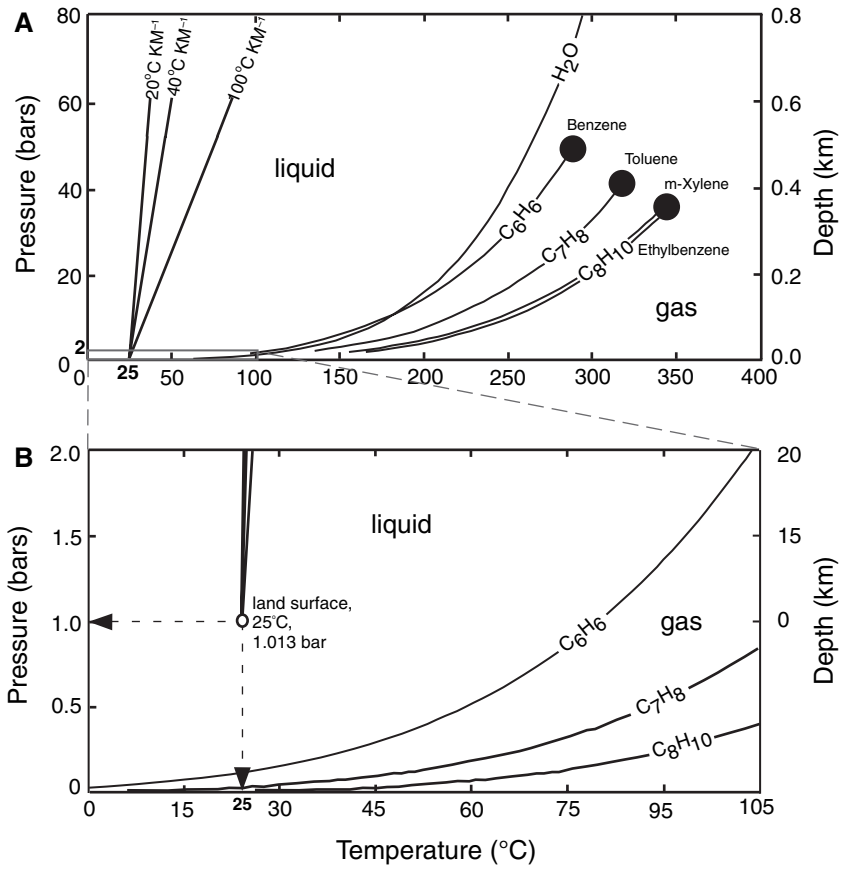

Fig. 2. (A) BTEX and water boiling curves and critical points (dots) (after Helgeson *et al.* 1998). One bar is equivalent to approximately 10^5 Pa. (B) BTEX boiling curves at the near-surface temperature and pressure conditions (Aljoe *et al.* 1986). Three representative geotherms of sedimentary basins are superimposed onto each plot.

compositions can be significantly modified by biodegradation (Kuo 1994; Huang *et al.* 2004), as bacteria have been found in crude oil, oil field waters and sediments up to a depth of 4200 m and can occur at all depths above a hydrocarbon deposit (Saunders *et al.* 1999; Schumacher 1999). In the deep subsurface, bacterial populations which only consume hydrocarbons increase with increasing proximity to an oil deposit and biodegradation is considered an important factor controlling the fate of hydrocarbons at depth (Price 1985). Aerobic biodegradation of hydrocarbons has been extensively studied (Atlas 1984), while important anaerobes such as iron-reducing, sulfate-reducing, and denitrifying bacteria also exist in the subsurface and benzene anaerobic biodegradation is linked to methanogenesis (Kazumi *et al.* 1997; Burland & Edwards 1999). Recent work further suggests that anaerobic biodegradation is the dominant mechanism in hydrocarbon consumption, even in shallow oil reservoirs (<500 m) containing fresh water (Head *et al.* 2003).

In this study, the effect of groundwater flow on soluble benzene migration in sedimentary basins is quantitatively assessed. Using an idealized basin cross-section, a coupled groundwater flow and heat transfer model simulates basin-scale topographically driven flow and temperature. A coupled mass transport model simulates water washing of benzene from an oil reservoir and the concurrent transport by groundwater. We focus on benzene because among BTEX compounds, it is the most mobile (Odermatt 1994), least sorptive (Patrick & Barker 1985; Lipson & Siegel 2000) and the most resistant to anaerobic biodegradation (Chapelle *et al.* 1993). A sensitivity study is carried out by varying the hydrological and geochemical properties of the model basin to determine their influence on soluble benzene migration. In particular, the permeability of the cap rock (rocks of lower permeability that lie above the oil reservoir) is varied, resulting in significant variations in the regional groundwater flow patterns. The sensitivity study is constructed to address the following questions:

- What aquifer and geochemical parameters control soluble benzene transport?
- What is the threshold permeability of the cap rock above an oil field that restricts upward benzene migration towards the surface?
- Under what conditions can benzene be found in measurable concentration (>0.01 ppm) in springs or exploration wells adjacent to an oil field?
- Can diffusion explain the observed distances where benzene is found in formation water adjacent to known oil reservoirs?

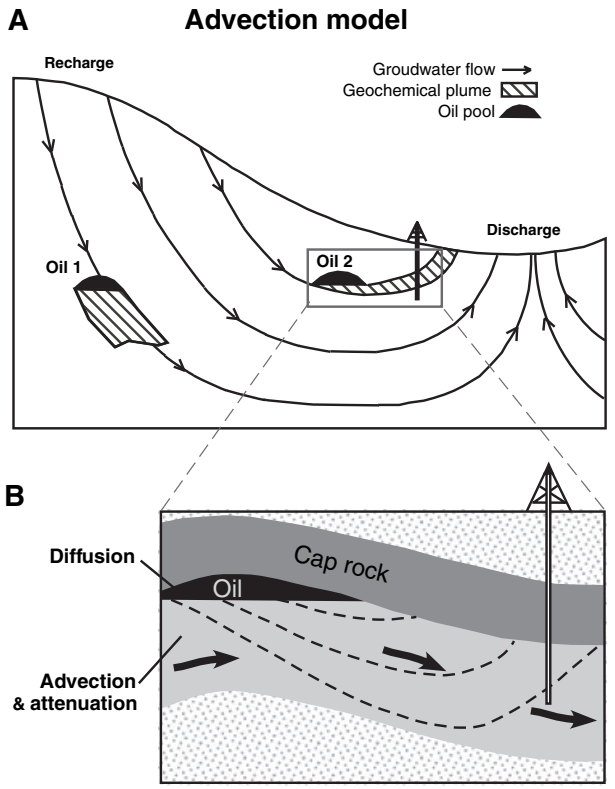

Fig. 3. (A) A schematic diagram of oil reservoirs in an active groundwater flow system (after Machel & Burton 1991). Due to attenuation, the hydrocarbon plume emanating from oil pool 1 is not able to reach the surface. (B) A schematic diagram of the coupled benzene transport process modeled in this study. Benzene diffusion occurs within the oil reservoir; its advective/dispersive transport occurs in the groundwater.

The remainder of the paper is organized into five sections. First, we describe the transport equations and the numerical models used. Next we present a sensitivity study in which the cap rock permeability, the benzene mass transfer coefficient, the location of the oil reservoir and the biodegradation rate constant are systematically varied. The relative importance of diffusion versus advection is then addressed. The results are summarized in Discussion and Conclusions. At the end of the paper, future research directions are identified.

MATHEMATICAL MODEL

Conceptual model

A mathematical model is developed to represent the transport and attenuation of dissolved benzene in a sedimentary basin. The model solves coupled steady-state groundwater flow and heat transfer equations to calculate hydraulic head, groundwater flow rate and temperature in the basin. A transient solute transport model is used to represent advective–dispersive benzene transport by groundwater and its attenuation via retardation and biodegradation. This transport model is coupled at the oil–water contact to a diffusion model which represents benzene migration within an oil reservoir. Benzene mass transfer across the oil–water phase boundary is described by a first-order Newtonian mass transfer law. A thermodynamic model is used to compute the *in-situ* equilibrium partition coefficient for the mass transfer of benzene from the oil phase to the aqueous phase.

Mathematical equations

The governing equation describing the steady-state variable-density groundwater flow within a sedimentary basin is given by (Garven & Freeze 1984):

$$\nabla \cdot [\rho_f \vec{q}] = 0 \tag{1a}$$

where ∇ is a gradient operator, '·' represents the inner product, ρ_f is the density of groundwater, $\vec{q}$ is the Darcy flux. Darcy's law for variable-density flow is given by:

$$\vec{q} = -\mu_r \mathbf{K} \nabla (h + \rho_r z) \tag{1b}$$

where h is the hydraulic head, ρ_r is the relative density $[\rho_r = (\rho_f - \rho_0)/\rho_0]$, μ_r is the relative viscosity ($\mu_r = \mu_0/\mu_f$), μ_f is the dynamic viscosity of groundwater, ρ_0 and μ_0 are the reference density and viscosity of fresh water defined at 20°C and 1.01×10^5 Pa, $\mathbf{K}$ is the hydraulic conductivity tensor, which is related to the intrinsic permeability tensor $\mathbf{k}$ at the reference density and viscosity ($\mathbf{K} = (\rho_0 g/\mu_0)\mathbf{k}$). With equation (1), groundwater flow is driven by both the topographic relief of the regional water table and the fluid density gradient due to temperature variations in the basin. For a two-dimensional problem, the hydraulic conductivity $\mathbf{K}$ is calculated based on the principal components and the sedimentary layer dip:

$$\begin{aligned} K_{xx} &= K_{\max} \cos^2\theta + K_{\min}^2 \sin\theta \\ K_{zz} &= K_{\max} \sin^2\theta + K_{\min} \cos^2\theta \\ K_{xz} &= K_{zx} = (K_{\max} - K_{\min}) \sin\theta \cos\theta \end{aligned} \tag{2}$$

where $K_{\max}$ is the maximum principal conductivity, $K_{\min}$ is the minimum principal conductivity, and θ is the dip angle of a hydrostratigraphic unit relative to the horizontal plane. K_{xx}, K_{zz}, K_{zx}, K_{xz} are the components of $\mathbf{K}$. The minimum principal conductivity is typically assumed to be perpendicular to the bedding plane.

For variable-density groundwater flow, stream function is used to visualize the transport directions (Appold and Garven, 1999):

$$\nabla \cdot \left[\frac{\mathbf{K}}{|\mathbf{K}|} \frac{1}{\rho_f \mu_r} \nabla \Psi \right] = -\frac{\partial \rho_r}{\partial x} \tag{3a}$$

where $|\mathbf{K}|$ is the determinant of $\mathbf{K}$, Ψ is a mass-based stream function which is related to the Darcy flux via the

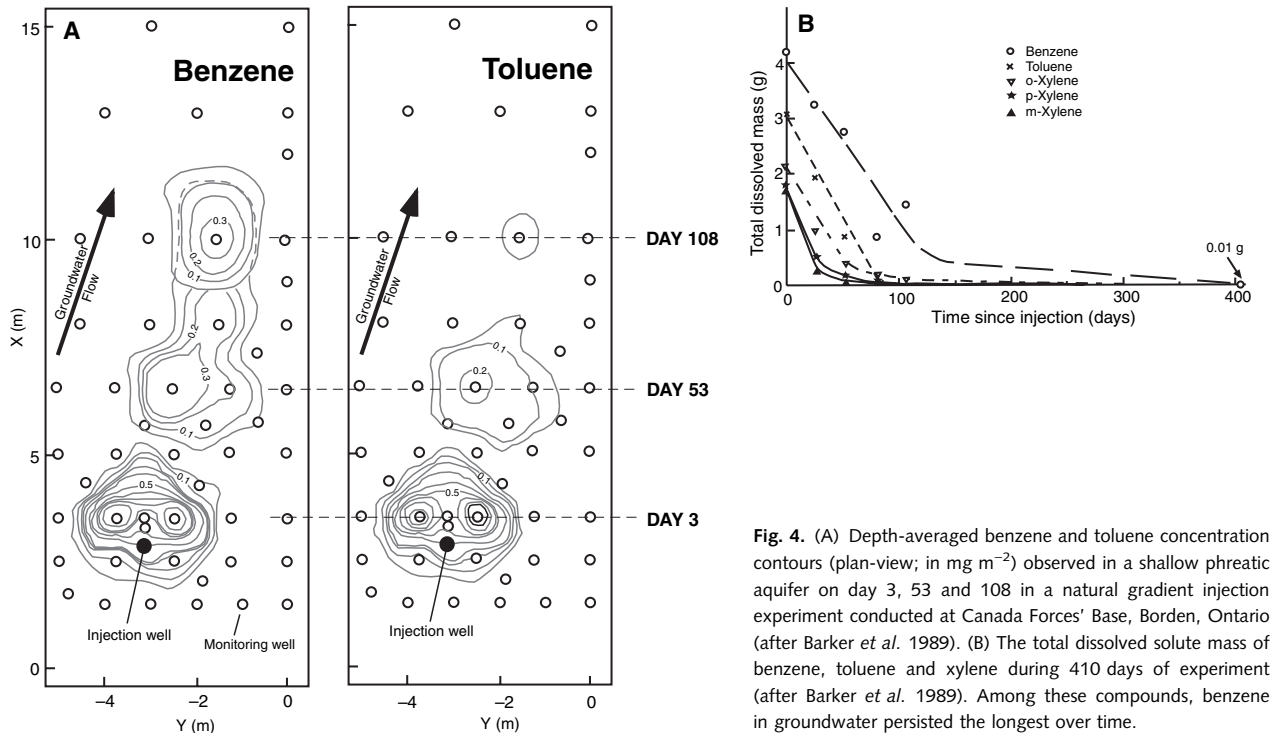

Fig. 4. (A) Depth-averaged benzene and toluene concentration contours (plan-view; in mg m^{-2}) observed in a shallow phreatic aquifer on day 3, 53 and 108 in a natural gradient injection experiment conducted at Canada Forces' Base, Borden, Ontario (after Barker *et al.* 1989). (B) The total dissolved solute mass of benzene, toluene and xylene during 410 days of experiment (after Barker *et al.* 1989). Among these compounds, benzene in groundwater persisted the longest over time.

fluid density ρ_f:

$$\rho_f q_x = -\frac{\partial \Psi}{\partial z}; \qquad \rho_f q_z = \frac{\partial \Psi}{\partial x} \tag{3b}$$

q_x and q_z are the components of the Darcy velocity $\vec{q}$ in the x and z directions, respectively.

Heat transfer can be effected by conduction and convection (Bear 1988). The governing equation for steady-state heat transfer is given by:

$$\nabla \cdot (\boldsymbol{\lambda} \nabla T) = \rho_f c_f \vec{q} \cdot \nabla T \tag{4}$$

where λ is the thermal conduction–dispersion tensor, T is the temperature of groundwater, c_f is the specific heat capacity of groundwater. On the right-hand side of equation (4), the '·' represents the inner product of $\vec{q}$ and ∇T (gradient of T is a vector). Equation (4) implicitly assumes that solid phase is in thermal equilibrium with fluid phase, a reasonable assumption for most sedimentary basin environments. Effects of anisotropy and heterogeneity in the thermal properties can be accounted for through the components (λ_{xx},λ_{zz},λ_{xz},λ_{zx}) of the thermal dispersion–conduction tensor $\boldsymbol{\lambda}$:

$$\begin{aligned}
\lambda_{xx} &= \rho_f c_f \frac{q_x^2}{|\vec{q}|}\alpha_L + \rho_f c_f \frac{q_z^2}{|\vec{q}|}\alpha_T + \lambda_f^{\phi}\lambda_s^{1-\phi} \\
\lambda_{zz} &= \rho_f c_f \frac{q_x^2}{|\vec{q}|}\alpha_T + \rho_f c_f \frac{q_z^2}{|\vec{q}|}\alpha_L + \lambda_f^{\phi}\lambda_s^{1-\phi} \\
\lambda_{xz} &= \lambda_{zx} = (\alpha_L - \alpha_T)\frac{q_x q_z}{|\vec{q}|}\rho_f c_f
\end{aligned} \tag{5}$$

where α_L and α_T are the longitudinal and transverse dispersivities, and λ_f and λ_s are the thermal conductivity of the fluid and solid phases, respectively. $|\vec{q}|$ is the magnitude of the Darcy flux. Equation (4) describing heat transfer is coupled to the groundwater flow equation (1) through an equation of state in the form of fitted polynomials to relate the fluid density and viscosity to its temperature and pressure (Kestin *et al.* 1981).

Aqueous benzene transport by groundwater is controlled by advection, hydrodynamic dispersion, diffusion and attenuation (Zheng & Bennett 1995):

$$R\frac{\partial C_w}{\partial t} = \nabla \cdot [\mathbf{D}\nabla C_w] - \vec{v} \cdot \nabla C_w - \lambda C_w \tag{6}$$

where R is a retardation factor which describes benzene sorption and de-sorption onto sediment particles, C_w is the aqueous benzene concentration, $\vec{v}$ is the groundwater velocity ($\vec{v} = \vec{q}/\phi$), ϕ is porosity, λ is a first-order biodegradation rate constant, $\mathbf{D}$ is a hydrodynamic diffusion–dispersion tensor with components defined as (Bear 1988):

$$\begin{aligned}
D_{xx} &= \frac{v_x^2}{|\vec{v}|}\alpha_L + \frac{v_z^2}{|\vec{v}|}\alpha_T + D_{aq}^e \\
D_{zz} &= \frac{v_x^2}{|\vec{v}|}\alpha_T + \frac{v_z^2}{|\vec{v}|}\alpha_L + D_{aq}^e \\
D_{xz} &= D_{zx} = (\alpha_L - \alpha_T)\frac{v_x v_z}{|\vec{v}|}
\end{aligned} \tag{7}$$

where v_x and v_z are the horizontal and vertical components of $\vec{v}$, respectively, D_{aq}^e is an effective diffusion coefficient of

aqueous benzene in the porous medium, and $|\vec{v}| = \sqrt{v_x^2 + v_z^2}$ is the magnitude of the groundwater velocity.

Laboratory and field experiments as well as numerical modeling studies have been conducted to estimate the BTEX biodegradation rate constant in shallow groundwater flows and soils (e.g. Sudicky & MacQuarrie 1989; Borden *et al.* 1997a,b; Landmeyer *et al.* 1998; Lu *et al.* 1999; Ma *et al.* 1999; Suarez & Rifai 2004). For benzene, the first-order biodegradation rate constant (λ) ranges from 0.0002 to 0.05 day^{-1} for aerobic biodegradation and 0.0001 to 0.03 day^{-1} for anaerobic biodegradation. These rate constants are often site-specific and sometimes are constrained by the mixing rate, the diffusivity of oxygen, and the availability of nutrients. A retardation factor (R) of benzene has been estimated to be 1.1 for a sandy aquifer (Patrick & Barker 1985). R is further a function of the sediment organic carbon content. No sorption can occur if the sediments in contact with benzene do not possess any organic matter (G. Lu, 2000, personal communication). Compared with the biodegradation rate constant that can vary by several orders of magnitude, the retardation factor appears to be secondary in limiting the extent of benzene transport. In this study, most of the benzene transport occurs at depths greater than 1 km where anaerobic biodegradation most likely dominates. Although the biodegradation rate constant in the deep subsurface has not been directly measured, e.g. bacteria that can degrade hydrocarbons *in situ* have not been isolated, Head *et al.* (2003) suggest a first-order rate constant of 10^{-6}–10^{-7} $year^{-1}$ for a reservoir temperature range of 60–70°C. The anaerobic biodegradation rate constant further decreases with increasing temperature (Head *et al.* 2003). Clearly, hydrocarbon biodegradation at depths may not be as active as it is near the surface. In this study, the rate constants estimated for the shallow flow systems and the deep oil fields are used as the upper and lower limit in the modeling of benzene biodegration, respectively.

Benzene migration within the oil reservoir is represented with a diffusion model:

$$\frac{\partial C_0}{\partial t} = \nabla \cdot [D_{\text{oil}}^{\text{e}} \nabla C_{\text{oil}}] \tag{8}$$

where $D_{\text{oil}}^{\text{e}}$ is an effective diffusion coefficient of the oil-phase benzene; C_{oil} is the concentration of benzene in oil. Note that equation (8) differs with equation (6) in several respects: first, no retardation of benzene occurs within the oil reservoir ($R = 1$); second, bulk advective movement of benzene within the oil reservoir is considered negligible. The oil itself is considered immobile (or $\vec{v}_{\text{oil}} = 0$) – a reasonable assumption for most structurally trapped reservoirs that are not being produced, **D** in equation (6) is thus reduced to the effective diffusion coefficient $D_{\text{oil}}^{\text{e}}$; third, no benzene sources or sinks exist within the oil reservoir ($\lambda = 0$). The relationship between the effective diffusion coefficient D^{e} (D_{aq}^{e} or $D_{\text{oil}}^{\text{e}}$) and the diffusion coefficient D (D_{aq} or D_{oil}) is given by Parker (1989) assuming isotropic diffusion in porous media:

$$D_{\text{e}} = \phi^{0.33} S^{2.33} D \tag{8a}$$

where S is the saturation ratio of a fluid. The diffusion coefficient (D_{aq} or D_{oil}) are computed according to the equations of state given by Reid *et al.* (1987).

Benzene diffusion within the oil reservoir and its advective–dispersive transport by groundwater are coupled at the oil–water contact. Benzene partitions out of the oil into the water, as aqueous benzene concentration near the phase boundary is continuously lowered via miscible transport (Lafargue & Thiez 1996). This process is also called water washing as lighter and more soluble hydrocarbons are preferentially removed from oils. As a result, a concentration gradient is established within the oil reservoir, which drives benzene diffusion within oil. To represent the coupled transfer process, the numerical grids for each fluid phase are linked at the oil reservoir boundary (Fig. 5). In this study, this boundary layer is assumed to be thin relative to the thickness of the oil column. Oil droplets are formed at the phase boundary, characterized by an average length l_{c}. At the boundary layer, the saturation ratio of oil (S_{oil}) or that of water ($S_{\text{w}} = 1 - S_{\text{oil}}$) is not known, and is a parameter varied in our sensitivity study. Beyond the boundary layer, the groundwater and the oil are assumed to fully saturate the pores within their respective domains.

Benzene mass transfer across the phase boundary is described using a first-order Newtonian mass transfer law, assuming equilibrium partitioning of benzene at the oil–water contact (Powers *et al.* 1991):

$$C_6H_{6(\text{oil})} = C_6H_{6(\text{aq})} \tag{9}$$

$$J = -k_{\text{f}}[C_{\text{w}} - C_{\text{I}}] \tag{9a}$$

$$C_{\text{I}} = C_{\text{oil}} \cdot \Gamma \tag{9b}$$

where C_6H_6 is the chemical formula for benzene and the subscripts 'oil' and 'aq' represent the oil and aqueous phase, respectively; k_{f} is a mass transfer coefficient; C_{w}, C_{oil} are the bulk aqueous and oil-phase benzene concentration (in ppm), respectively; C_{I} is the aqueous benzene concentration at the phase boundary (in ppm); J is benzene mass flux. To conserve mass, J is negative on the flux boundary for the oil reservoir model and equal and positive on the flux boundary for the groundwater model. Γ (ppm/ppm) is the equilibrium partition coefficient. The above mass transfer law assumes that dissolved benzene reaches equilibrium quickly relative to its transfer across the phase boundary, as the *in-situ* partitioning of aromatics from oil

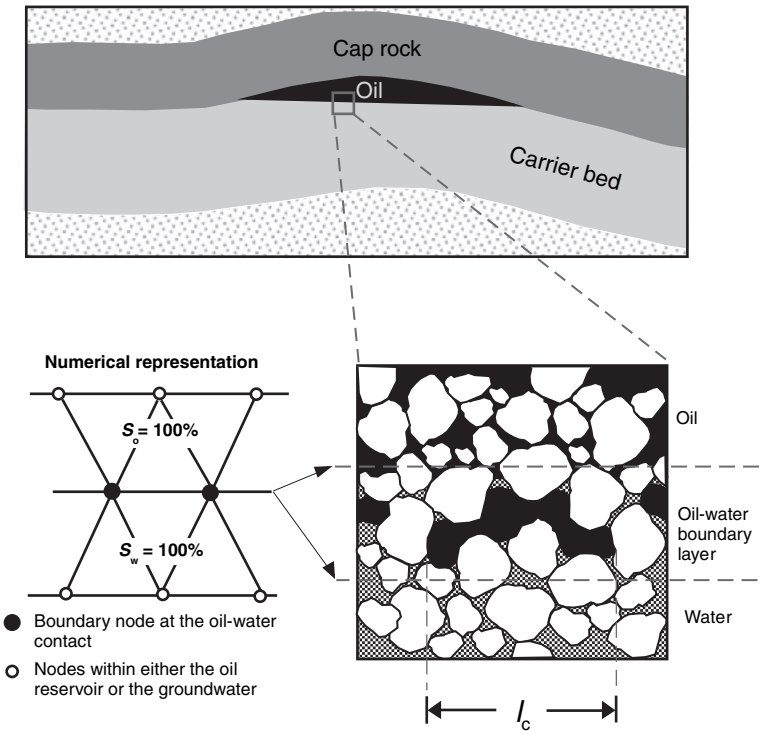

Fig. 5. A schematic diagram of an oil–water contact between an oil reservoir and an underlying carrier bed (modified from Powers *et al.* 1991). Oil droplets are formed at the phase boundary, characterized by a length scale l_c. Numerically, the oil–water contact is represented by the boundary nodes (solid circles) of the oil reservoir. Oil and water fully saturates the pore spaces on either side of the contact.

to oil-field waters has been found to occur within minutes (Larter *et al.* 1997).

For reaction (9), the mass-action law can be written as:

$$K = K(T,P) = \frac{a_{\rm aq}}{a_{\rm oil}} = \frac{\gamma_{\rm aq}}{f_{\rm oil}} \cdot \frac{m_{\rm aq}}{X_{\rm oil}} = \frac{\gamma_{\rm aq}}{f_{\rm oil}} \Gamma^*; \quad \Gamma^* = \frac{m_{\rm aq}}{X_{\rm oil}} \tag{10}$$

where $a_{\rm aq}$ and $a_{\rm oil}$ are the activities of aqueous- and oil-phase benzene, respectively; $m_{\rm aq}$ is the molality of aqueous benzene; $X_{\rm oil}$ is the mole fraction of oil-phase benzene; $\gamma_{\rm aq}$ and $f_{\rm oil}$ are the corresponding activity coefficients; Γ^* is the equilibrium partition coefficient defined in units of molality/mole fraction, Γ^* can be converted to Γ given an average molecular weight of oil; K is the temperature- and pressure-dependent equilibrium constant of the reaction, which can be independently calculated from standard state properties of benzene, see below. From (10), the partition coefficient Γ^* can be obtained by dividing K by the ratio of the activity coefficients ($\gamma_{\rm aq}/f_{\rm oil}$). As benzene found in crude oil and formation water is usually dilute, the activity coefficients can be approximated by unity (Prausnitz *et al.* 1999). Γ^* can then be approximated by the equilibrium constant K, or

$$m_{\rm aq} = KX_{\rm oil} \tag{11}$$

By converting $m_{\rm aq}$ to $C_{\rm I}$ (ppm) and $X_{\rm oil}$ to $C_{\rm oil}$ (ppm), equation (11) is reduced to equation (9b). In a binary system where pure benzene is in equilibrium with water, $X_{\rm oil} = 1$, and from equation (11), K is equivalent to the *pure liquid solubility* in molality units ($m_{\rm aq}^{\rm solubility}$)

$$K = m_{\rm aq}^{\rm solubility} \tag{12}$$

equation (11) is then reduced to Raoult's law

$$m_{\rm aq} = m_{\rm aq}^{\rm solubility} X_{\rm oil} \tag{13}$$

which governs the solubility of ideal organic mixtures in water (e.g. Banerjee 1984; Chrysikopoulos & Lee 1998).

Effect of high salinity

While dilute, aqueous benzene has an activity coefficient close to unity. In high-salinity formation waters, aqueous benzene has an activity coefficient slightly greater than unity (which results in a slight salting-out effect), due to the fact that aqueous benzene is neutral. Indeed, for neutral aqueous species (Helgeson 1969, equation 36 and Fig. 3), $\log_{10}\gamma = \sigma I$, where $\sigma \approx 0.04$ for the temperature interval of 25–125°C. Thus, for a concentrated 1-molal brine, $\log_{10}\gamma = 0.04 \times 1.0 = 0.04$ and $\gamma = 1.096$, which would only bring about a 10% decrease in solubility.

Calculation of the equilibrium constant

The equilibrium constant K for equation (9) is calculated for a given temperature and pressure range from the standard-state thermodynamic properties of the aqueous- and liquid-phase benzene (Shock & Helgeson 1990; Helgeson *et al.* 1998; Richard & Helgeson 1998), using the computer program SUPCRT92 (Johnson *et al.* 1992). The

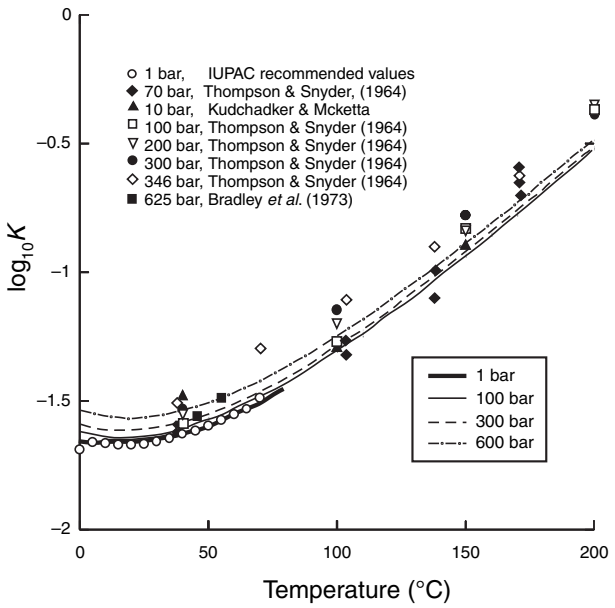

Fig. 6. The equilibrium constant K (curves; in log scale) computed with SUPCRT92 as a function of temperature and pressure for the aqueous benzene dissolution reaction. Also plotted for comparison are the experimental benzene pure liquid solubilities (dots) measured under different temperature and pressure conditions (all works referenced in the plot were compiled into the IUPAC solubility data series, 1989).

calculated values of K are compared with the experimental benzene pure liquid solubilities (IUPAC solubility series, 1989) in Fig. 6. For a temperature range of 0–200°C and a pressure range of 1–600 bar bracketing the known conditions in oil reservoirs, the equilibrium constant (curves; in log scale) fit the experimental solubilities (dots) within 0.1 log unit. K is sensitive to the change in temperature, but not sensitive to the change in pressure. As temperature increases, K increases, and more benzene partitions into the aqueous phase.

Calculation of the mass transfer coefficient

The mass transfer coefficient k_f at the oil–water contact is computed with an empirical relationship (Powers *et al.* 1991):

$$\begin{cases} S_h = S_c^{0.33}(\phi S_w)^{-1}(0.765R_e^{0.18} + 0.365R_e^{0.614}) \\ R_e = l_c|\vec{q}|\rho_w/\mu_w \\ S_c = \mu_w/D\rho_w \\ k_f = S_h D/l_c \end{cases} \quad (14)$$

where S_h is the Sherwood number (dimensionless); R_e is the Reynolds number (dimensionless); S_c is the Schmidt number (dimensionless); D and S are the benzene diffusion coefficient and water saturation at the interphase, respectively. Equation (14) is chosen among several relationships, but is valid for all Reynolds numbers to account for a wider range of variations in groundwater velocity. Equations (9)–(14) indicate that benzene mass transfer is influenced not only by the equilibrium constant of the dissolution reaction, but also by the groundwater flow rate, the water saturation and the characteristic oil length at the interphase.

Numerical methods

The mathematical equations (1), (3), (4), (6), and (8) describing the steady-state groundwater flow, the stream function, the heat transfer and the transient coupled benzene transport are solved numerically with the finite element method using three-node triangular elements. A cross-sectional hydrostratigraphy is discretized using the Argus^{TM} mesh generation software so that the geometric configuration of the stratigraphic units is honored. The modified method of characteristics (MMOC) is used to solve the transient transport equations. This approach has some decisive advantages over classical finite element solution methods for advection dominated problems (Zheng & Bennett 1995). With the finite element approximations, the above equations are transformed into sets of linear equations which are then solved using a direct Gaussian elimination solver. The transport model in the basin is simulated for 5 Ma using a high-performance IBM SP supercomputer. This chosen time span ensures that a significant portion of the oil is waterwashed while dissolved benzene is able to reach the water table in the regional groundwater discharge areas.

Initial and boundary conditions

For the steady-state groundwater flow equation, a specified head equal to the water table elevation is assigned to the top boundary (Tóth 1963). No-flow boundaries are imposed on the sides and the bottom of the basin. For the heat transfer equation, a specified temperature of 15°C is assigned to the top boundary representing the average annual surface temperature of the basin. A constant heat flux of 60 mW m^{-2} is assigned at the base while the sides of the basin are assumed to be insulated. For the transient solute transport equation, the initial benzene concentration everywhere in the basin is zero. A constant zero concentration is also assigned to the top boundary except along the outflow area where an advective flux is specified. The sides and the bottom of the basin are no-flux boundaries. An internal flux boundary is additionally assigned at the oil–water contact. Benzene mass in-flux for the aqueous transport equation is calculated with equation (9). This same mass flux is imposed at the boundary of the diffusion model representing benzene transport within an oil reservoir. The initial benzene concentration within the oil reservoir is set at 1500 ppm, reflecting roughly a median benzene concentration found in many crude oils.

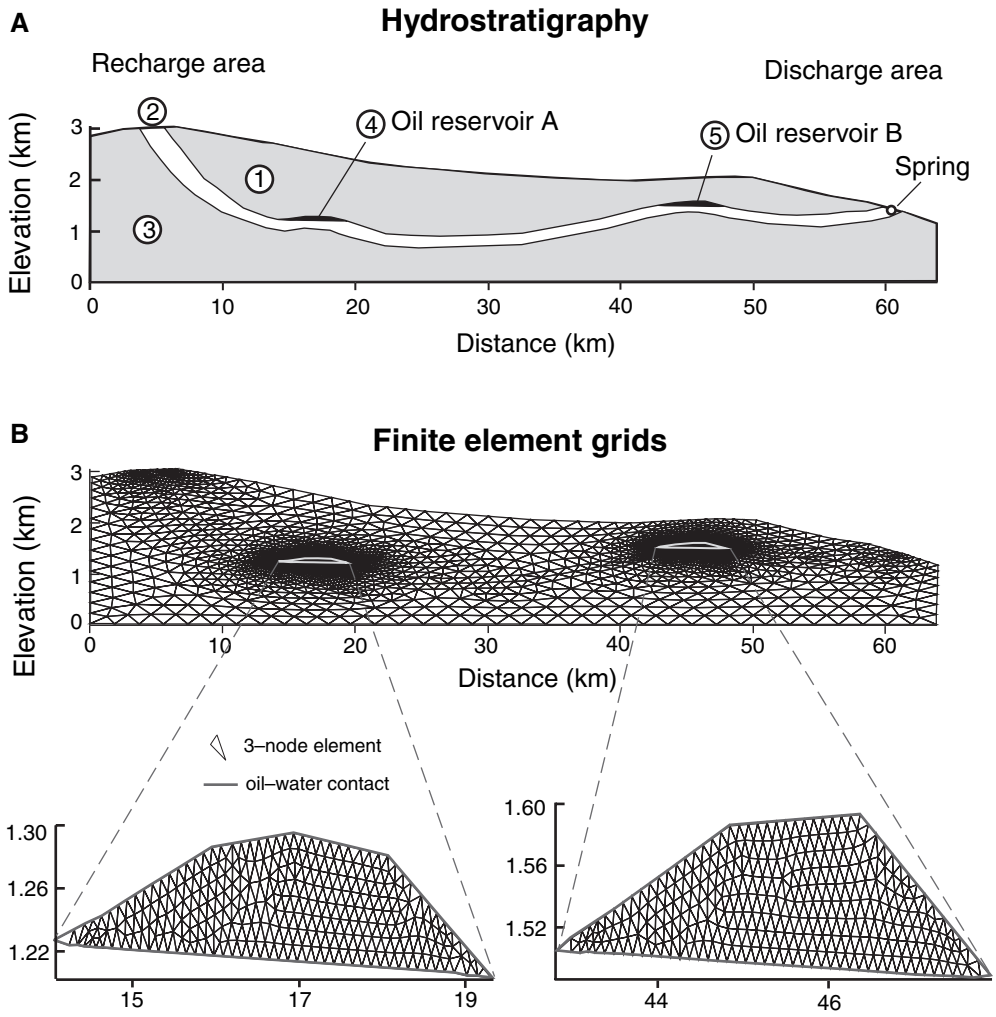

Fig. 7. (A) Model basin cross-section representing 5 hydrostratigraphic units: (1) an overlying confining unit (cap rock); (2) an aquifer; (3) an underlying confining unit; (4) oil reservoir A; and (5) oil reservoir B. The aquifer outcrops both at the highland recharge area and the lowland discharge area in the basin. (B) The numerical grids used for the basin and the oil reservoir models. The oil–water contact (gray outlines) corresponds to the boundary of the oil reservoir.

SENSITIVITY STUDY

Model configuration

To simulate groundwater flow, heat transfer and solute transport, a suite of numerical experiments is conducted using an idealized cross-section of a sedimentary basin with a simplified hydrostratigraphy (Fig. 7A). The model basin has a length of 64 km and a maximum depth of 3 km. Five hydrostratigraphic units are represented – an aquifer in the middle, an overlying confining unit (cap rock), an underlying confining unit and two oil reservoirs. The oil reservoirs are located within two stratigraphic traps of the aquifer. The size of the reservoirs ranges from 5 to 6 km in length and 80–100 m in thickness. Oil is assumed to have migrated into its current location from an underlying source rock; petrophysical properties of the reservoirs are the same as those of the aquifer. A spring boundary condition is specified where the confined aquifer meets the land surface. Finite element grids representing both the basin and the reservoirs are shown in Fig. 7B. The basin grid has 3329 nodes and 6529 elements; oil reservoir A has 296 nodes and 494 elements; oil reservoir B has 318 nodes and 540 elements. To represent the coupled mass transport process, these grids are linked at the oil–water contact where benzene mass fluxes for the shared nodes are calculated.

The hydrological and thermal parameters assigned to the aquifer and the confining units in the model basin are listed in Table 2. These properties are chosen based on the typical values estimated for basin-scale topographically driven groundwater flow systems (Garven 1989; Jury *et al.* 1991) and are shared to all simulation runs. In many respects, the model basin is similar in geometry and rock

Table 2 Hydrologic and thermal properties assigned to the hydrostratigraphy of the model basin.

Units	$\log_{10} k_x$ (m^2)	$\log_{10} k_z$ (m^2)	Porosity	λ_s (W m^{-1} °C^{-1})	λ_f (W m^{-1} °C^{-1})	c_f (J kg^{-1} °C^{-1})	α_L (m)	α_T (m)
Upper confining unit (cap rock)	−17	−18	0.2	2.0	0.59	4180.0	10.0	1.0
Aquifer	−14	−15.3	0.1	3.1				
Lower confining unit	−18	−19	0.05	2.0				

k_x/k_z are the principal permeabilities of the hydrostratigraphic units; λ_s and λ_f are the thermal conductivities of the rock and the fluid, respectively; C_f is the heat capacity of the groundwater; α_L and α_T are the longitudinal and transverse dispersivities assigned to the heat transfer and solute transport equations.

properties to many areas of the Colorado plateau region where basin-scale hydrodynamics is dominated by gravity-driven groundwater flow (e.g. Hanshaw & Hill 1969; Walvoord *et al.* 1999; Zhu 2000). A base model for the sensitivity study is presented first using parameters listed in Table 2. The permeability contrast between the aquifer and the overlying cap rock is then varied. The mass transfer coefficient is varied next by choosing different oil characteristic length and water saturation, after which the oil reservoir closer to the spring is simulated. The effect of biodegradation is also evaluated. The simulation parameters varied in the sensitivity study are summarized in Table 3.

Table 3 Hydrological and biogeochemical parameters varied in the sensitivity study.

	$\log_{10} k_x$ (m^2)	$\log_{10} k_z$ (m^2)	l_c (m)	S_w	R	λ ($year^{-1}$)
Base model	−17	−18	1.0	0.5	1.0	0.0
Cap rock	−19	−20	1.0	0.5	1.0	0.0
permeability	−15	−16	1.0	0.5	1.0	0.0
Mass transfer	−17	−18	10.0	0.5	1.0	0.0
coefficient	−17	−18	0.1	0.5	1.0	0.0
	−17	−18	1.0	0.1	1.0	0.0
	−17	−18	1.0	0.9	1.0	0.0
Reservoir B	−17	−18	1.0	0.5	1.0	0.0
Attenuation	−17	−18	1.0	0.5	1.1	1.0×10^{-5}
	−17	−18	1.0	0.5	1.1	1.0×10^{-4}
	−17	−18	1.0	0.5	1.1	1.0×10^{-3}

k_x/k_z are the principal permeabilities of the cap rock; l_c: oil characteristic length; S_w: water saturation at the oil–water contact; R: retardation factor; λ: first-order biodegradation rate constant. When oil reservoir B is simulated, all parameters remain the same as those of the base model, but the location of the oil reservoir is different.

Base model simulation

In the base model, oil reservoir A is represented which is located 55 km away from the spring. About 100 iterations between the groundwater flow and heat transfer simulations are required before the hydraulic head, stream function and temperature across the basin are equilibrated (Fig. 8). Given the aquifer and thermal parameters assigned, groundwater in the basin is dominated by topography-driven flow from the areas of higher water table to the lowland discharge areas. Groundwater velocities are the highest within the aquifer, with a range of 0.2–2.0 m $year^{-1}$. The aquifer constitutes a preferential flow pathway through which most of the flow in the basin is concentrated. The recharge area is also marked by significantly cooler temperature where the temperature profile is deflected downwards by descending groundwater.

Benzene diffusion within the oil reservoir and its advective–dispersive transport by groundwater are then simulated using the computed steady-state groundwater velocity and temperature in the basin. The coupled mass transport model is run for 5 Ma. Due to the assumption that the oil reservoir has an oil saturation of 1.0, groundwater flow rate within the oil reservoir is set to zero. Although the stream function indicates that most of the groundwater concentrates within the aquifer before discharging at the spring, dissolved benzene exits the basin in more than one location. At the spring, benzene discharges in concentration ranging from 0.01 to 0.1 ppm. Despite the much lower groundwater velocities within the cap rock, e.g. average horizontal velocity is 6.0×10^{-4} m $year^{-1}$ and average vertical velocity is 3.0×10^{-4} m $year^{-1}$, upward benzene advection occurs through the cap rock in the center of the basin with significantly higher concentration (0.1–0.5 ppm). The highest concentration contour (0.5 ppm) occurs nearly vertically to the oil reservoir, indicating that advective transport by groundwater can also form the geochemical anomaly known as 'chimneys'. The lower concentration at the spring is mainly due to the diffusive losses across the confining beds.

The transport model is further run for longer simulation times to determine the time span for benzene to be flushed out of the oil reservoir. Given our assumption that no benzene source exists within the oil reservoir, it took 40 Ma to remove about half of the benzene. Using an effective diffusion coefficient of 10^{-11} m^2 sec^{-1} (approximately the magnitude of D_e computed with equation 8a), and an oil column height of 100 m, a similar time span of 30 Ma is estimated based on scale analysis of a one-dimensional

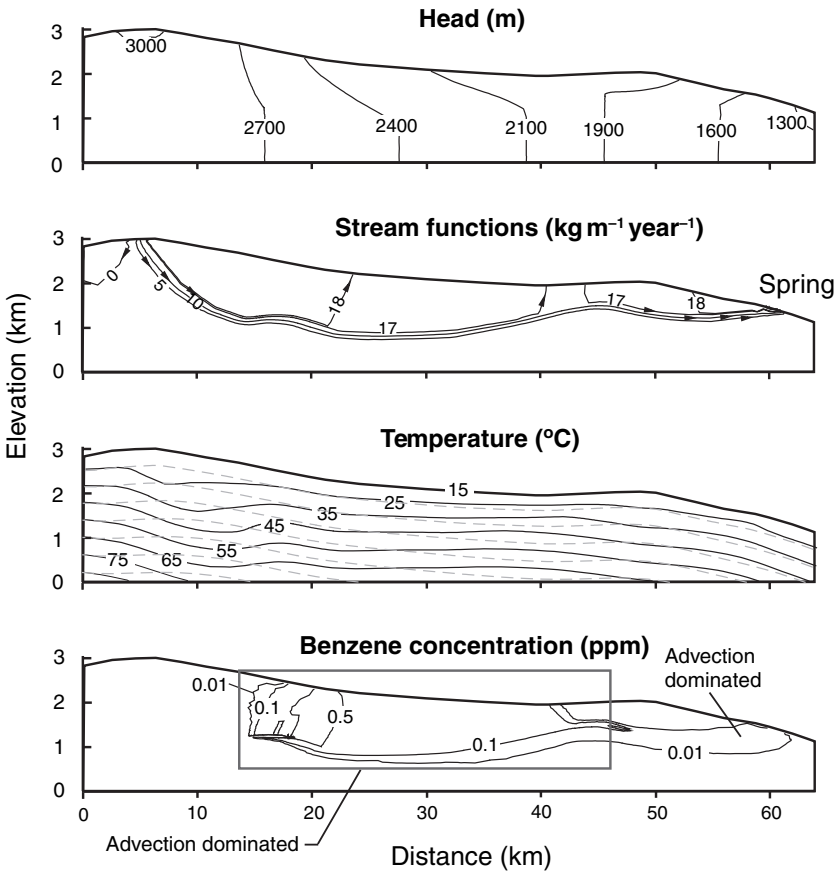

Fig. 8. The steady-state computed head, stream function and temperature in the base model simulation. Conductive temperature profiles are also plotted (dashed lines). Benzene concentration in the basin at the end of 5 Ma is shown.

diffusion model ($\Delta t = L^2/D_e$). These calculations indicate that roughly a diffusional time scale is required to flush benzene out of the oil reservoir.

Cap rock permeability

Hydraulic properties of the cap rock have been considered one of the important factors influencing separate phase hydrocarbon migration (Rostron & Tóth 1996). The effect of the cap rock permeability on soluble benzene migration is evaluated here. The cap rock is first assigned to be two orders of magnitude more permeable ($k_x = 10^{-15}$ m^2) than that of the base model ($k_x = 10^{-17}$ m^2), and in a second simulation, it is assigned a permeability two orders of magnitude less permeable ($k_x = 1.0^{-19}$ m^2). Permeability and porosity of the aquifer and the underlying confining unit remain the same as those of the base model.

When the cap rock permeability is relatively high ($k_x = 10^{-15}$ m^2), two local recharge/discharge cells form in the cap rock (Fig. 9A). Because of the lower permeability contrast between the aquifer ($k_x = 10^{-14}$ m^2) and the cap rock, the water table gradient has a strong control on the stream function. Regions of higher water table relief are characterized by groundwater recharge while adjacent areas of lower water table by discharge. Consequently, groundwater is no longer focused through the aquifer. Due to the higher groundwater velocities in the cap rock, the temperature profile is deflected significantly downward beneath the recharge area while the discharge area is characterized by higher temperature. When the cap rock permeability is set low ($k_x = 10^{-19}$ m^2), most of the groundwater in the basin is restricted to the aquifer and discharges only at the spring (Fig. 9B). Lower flow velocities within the cap rock also results in a less convective temperature profile.

Changes in the flow field in turn affect benzene transport in the basin. When the cap rock permeability is 10^{-17} m^2 (base model), benzene transport occurs both across the cap rock as well as within the aquifer to reach the spring (Fig. 8). With a more permeable cap rock ($k_x = 10^{-15}$ m^2), benzene transport is dominated by upward advection through the cap rock without reaching the spring (Fig. 9A). With a less permeable cap rock (10^{-19} m^2), benzene transport is dominated solely by advection through the aquifer as outlined by the 0.1 ppm concentration contour (Fig. 9B). In this case, benzene diffusion dominates within the cap rock and the underlying confining unit (0.01 ppm contours). Moreover, the

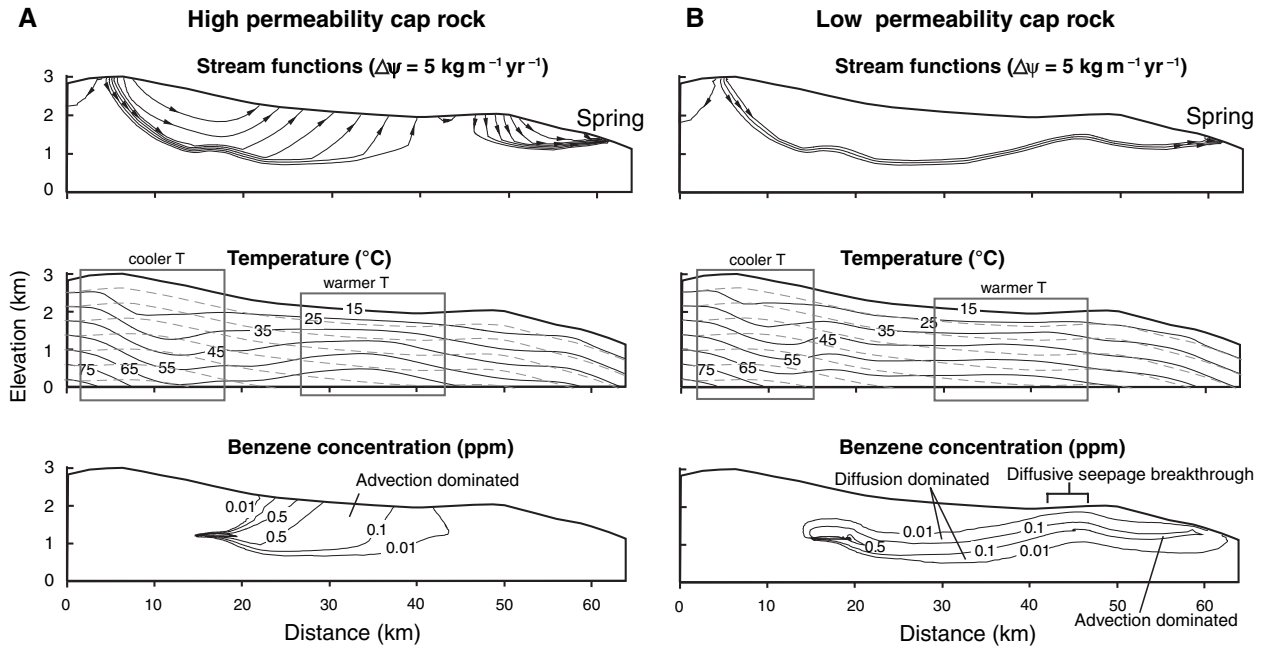

Fig. 9. The stream function, temperature, and benzene concentrations (5 Ma) in the basin, calculated when the permeability (k_x) of the cap rock is assigned to be (A) 10^{-15} m^2; and (B) 10^{-19} m^2.

travel time required for benzene to reach the water table above the oil reservoir varies significantly for all three models. It takes around 1.2 Ma for the base model benzene plume to reach the water table in the center of the basin, while it takes 80 000 years when the cap rock is more permeable. When the cap rock is less permeable, a diffusive benzene plume would reach the surface in approximately 6 Ma in the area where the confining bed is the thinnest. It is important to point out that the concentration plots presented in Figs 8 and 9 are 'snapshots', representing quasi-steady-state conditions. The initial plume development and final reservoir draining are not shown. Clearly, in this model setting where groundwater is driven by the regional water table gradient, the cap rock permeability not only influences the direction and extent of benzene transport, but it also determines the dominant transport mechanism within the cap rock and the speed of benzene migration.

Mass transfer coefficient

A mass transfer coefficient (k_f) is used to relate the concentration gradient to benzene mass flux across the oil–water contact. k_f is a function of groundwater density, viscosity, and velocity as well as water saturation (S_w), benzene diffusivity and characteristic oil length (l_c) at the interphase. Among these variables, only the water saturation and the oil length are unknown and thus subject to variation. To evaluate the impact of k_f on the coupled transport process, the oil length (l_c) is first varied by two orders of magnitude (Fig. 10). Using the same velocity and temperature fields as the base model, benzene transport is first simulated with an oil length of 10.0 m, and then an oil length of 0.1 m. As l_c increases, k_f decreases to approach the magnitude of the diffusion coefficient.

Minor differences exist among all models in terms of benzene concentration within the groundwater and the oil reservoir. The coupled mass transport process is not very sensitive to the mass transfer coefficient, probably due to the fact that benzene diffusion *within* the oil reservoir is rate-limiting. When k_f is large (or l_c is small) compared with the diffusivity of benzene in oil, benzene diffusion within the oil reservoir will eventually dominate. The amount of benzene crossing the interphase is limited by how fast benzene can diffuse within the oil to reach the oil–water contact, which in turn determines the amount of water washing over time. This is consistent with the diffusional time scale estimated for the base model. Moreover, given the same flushing time, higher diffusivities or hotter oils would result in more water washing of benzene. The results of benzene transport do not differ significantly among these three models, due to the fact that they use the same temperature field, thus the rate of benzene diffusion within the oil reservoir is the same. The water saturation (S_w) is also varied from 0.9 to 0.1 and the results of coupled benzene transport are comparable with those found by varying l_c (not shown).

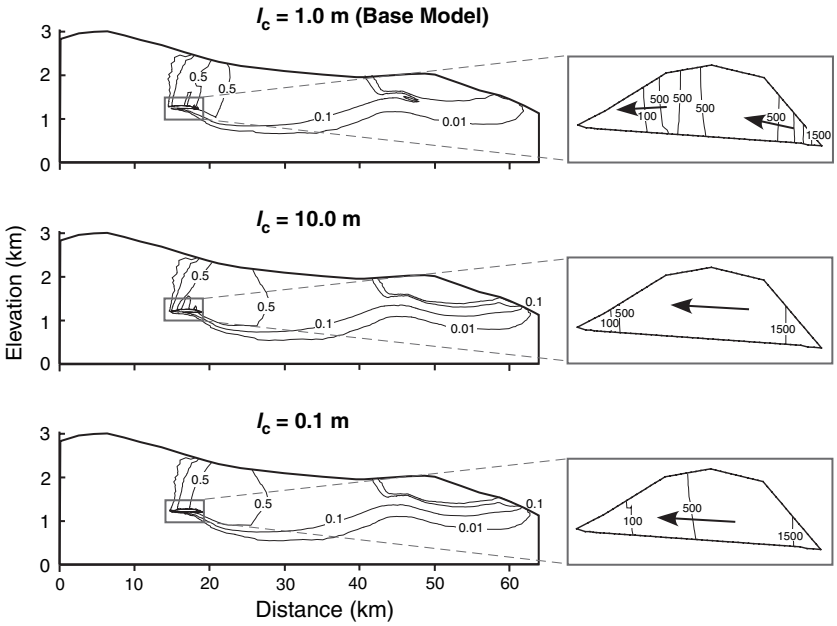

Fig. 10. Benzene concentration (in ppm) in the basin and the oil reservoir at 5 Ma.

Probably the most important observation is the effect of hydrodynamics on benzene concentration within the oil reservoir. In all three models, a strong lateral concentration gradient is established within the oil reservoir where benzene diffuses upstream in opposite direction to the ambient groundwater flow. Accordingly, a concentration boundary layer develops in the aquifer surrounding the oil reservoir. At the left boundary of the oil reservoir, benzene concentration in the oil phase is the lowest as the pristine groundwater first comes into contact with the oil. However, as the groundwater moves along the oil–water contact, benzene concentration in groundwater builds up, thus reducing the amount of mass transfer from the oil phase.

Location of the oil reservoir

When the oil reservoir B is simulated, the dominant flow direction within the cap rock above reservoir B is downward, preventing any upward migration towards the surface. Benzene transport occurs mainly in the aquifer and discharges only at the spring (Fig. 11A). Benzene transport from reservoir A in the base model simulation is also shown for comparison (Fig. 11A) and benzene concentration along the water table from both models are plotted (Fig. 11B). Groundwater advection had a significant impact on both the direction and distance that surface anomalies form in relation to the subsurface reservoir. In the base model where reservoir A is simulated, advection within the cap rock deflects the benzene plume towards the downstream side, resulting in an asymmetrical concentration profile along the water table. A significant surface anomaly forms over a 26 km length where the peak concentration (0.55 ppm) occurs at 3 km to the right of the oil reservoir, while little surface anomaly exists directly above the oil reservoir. This phenomena is similar to the 'edge effect' (geochemical anomalies observed in sediments lying directly above oil deposits) and confirms the proposition that ascending groundwater flow can act as a transport agent for hydrocarbons to form geochemical anomalies near the edge of oil deposits (North 1985). In the base model, a secondary anomaly also forms at the spring with a peak concentration of 0.06 ppm. The profile of this anomaly is nearly symmetrical and its width (about 3 km) is limited by the width of the aquifer outcropping at the spring. The magnitude of the spring concentration is also much smaller than that of the seepage concentration in the center of the basin. Clearly, higher groundwater velocities in the aquifer do not necessarily produce a stronger surface anomaly. A similar spring anomaly is produced when reservoir B is simulated. Due to the proximity of reservoir B to the spring, the peak concentration reaches 0.18 ppm, three times that due to transport from reservoir A. This anomaly lies 13.8 km downstream from reservoir B, while that due to reservoir A lies about 43 km downstream from reservoir A, roughly three times the distance to reservoir B. Therefore, the closer the reservoir is to the discharge area, the higher the concentration is at the spring. The above result also indicates an inverse linear relationship between the magnitude of peak benzene concentration in the spring and the distance to the reservoir. Note that this linear relationship may only apply when the reservoirs are influenced by the same regional flow system.

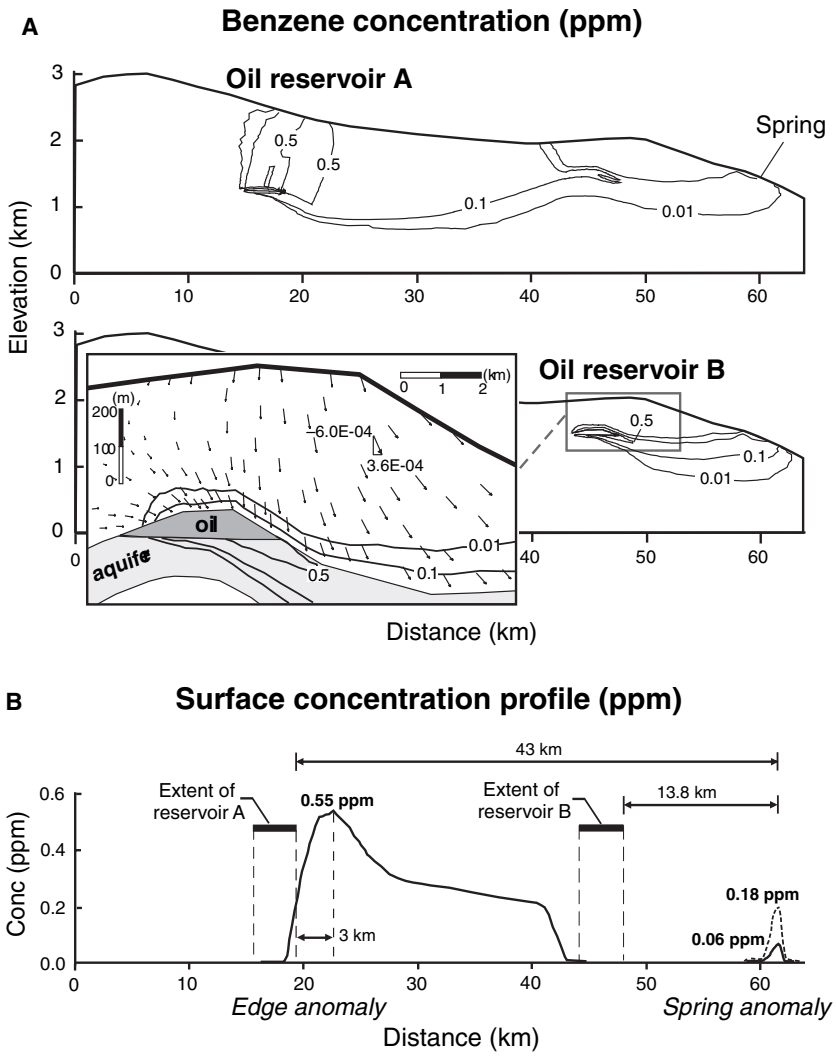

Fig. 11. (A) Benzene concentration (ppm) in the basin at 5 Ma. Two oil reservoirs are simulated: reservoir A (base model) and reservoir B. A close-up view of the groundwater flow within the cap rock above reservoir B is shown. (B) Benzene concentration along the water table from both models (reservoir A: lines; reservoir B: dashed lines). The location of the respective reservoir is also indicated.

Rate of attenuation

Light hydrocarbons such as BTEX attenuate as they migrate away from the subsurface oil reservoirs towards the surface (Price 1985). All previous benzene transport models in the sensitivity study do not represent its attenuation (Table 3). However, benzene measured from formation water adjacent to producing zones usually diminishes to below the detection limit within a lateral distance of 10 km. The maximum recorded distance from a known oil field is about 20 km (Burtell & Jones 1996). A sensitivity study is conducted by varying the biodegradation rate to observe its impact on benzene transport. The retardation rate, being of secondary importance, remains fixed at 1.1, assuming a constant rate of sorption/desorption along the transport path. Three biodegradation rate constants (λ) are used: 10^{-3}; 10^{-4}; 10^{-5} year^{-1}, ranging between the values estimated for the shallow flow systems and deeper oil fields. Benzene concentration in the basin at 5 Ma is plotted for all attenuation models and the base model (Fig. 12). As all four models utilize the same velocity field, the rate of biodegradation controls the transport distance. As the biodegradation rate increases, benzene transport becomes less extensive. When $\lambda = 10^{-5}$ year^{-1}, benzene reaches the spring in detectable concentration (>0.01 ppm), traveling a lateral distance of 45 km downgradient from the reservoir; when $\lambda = 10^{-4}$ and 10^{-3} year^{-1}, benzene diminishes to below detection at 15 and 2 km from the reservoir, respectively, and does not reach the spring in measurable concentration. Four hypothetical exploration wells are also placed in the basin, three intersecting the 0.1 ppm concentration contour, one intersecting the 0.01 ppm contour. The distance from the wells to the reservoir ranges from 2 to 30 km. Apparently, due to the difference in biodegradation rates assigned, the magnitude of benzene concentration measured in formation water alone cannot reveal the distance to the reservoir.

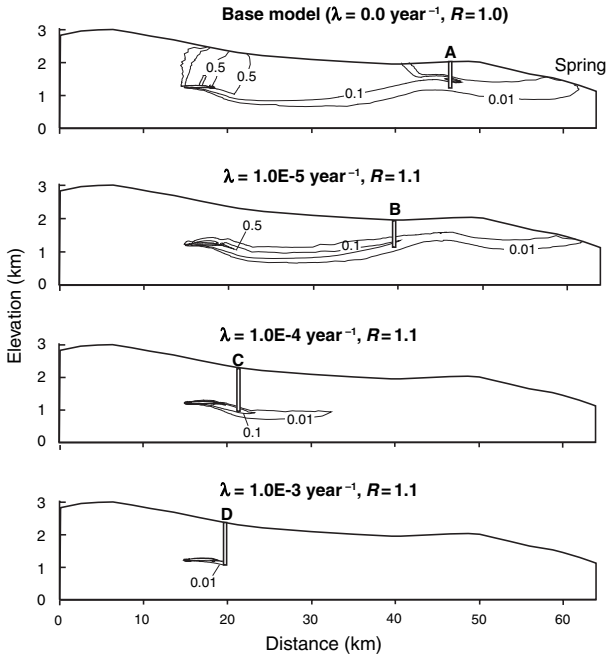

Fig. 12. Benzene concentration (ppm) in the basin at 5 Ma, with and without representing attenuation. Four hypothetical wells (A, B, C, D) are placed in the basin: A, B, C intersecting the 0.1 ppm contour; (D) intersecting the 0.01 ppm contour.

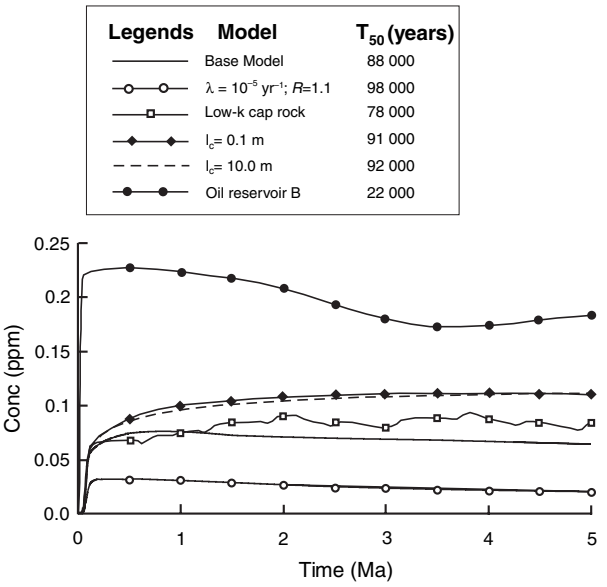

Fig. 13. Benzene breakthrough concentration (ppm) at the spring over 5 Ma for different simulations. The estimated breakthrough times (T_{50}) in years are also listed.

Solute breakthrough

For the previous simulations where benzene reaches the spring in detectable concentration, its breakthrough concentration at the spring through time is shown (Fig. 13). These simulations include the base model (solid line), the attenuation model with $\lambda = 10^{-5}$ year^{-1} and $R = 1.1$ (line with open circle), the model with low-permeability cap rock (line with open square), the models with different mass transfer coefficients (the dashed line and the line with solid diamonds) and the model representing reservoir B (line with solid circle). All solute breakthroughs display a distinctive 'S-shaped' profile indicating advective/dispersive transport. The breakthrough time (T_{50}) is defined as the time when benzene concentration reaches 50% of its quasi-steady-state level. Due to its proximity to the spring, benzene from reservoir B breakthroughs the earliest at 22 000 years, while T_{50} for all other models averages 90 000 years. By dividing the estimated T_{50} upon the distance benzene travels from its respective reservoir, the spatially averaged horizontal groundwater velocity ($\bar{v}_x$) within the aquifer is estimated to range from 0.5 to 0.7 m year^{-1}. Minor differences in T_{50} also exist among the models representing reservoir A. Notably, the effect of retardation ($R = 1.1$) can be seen from the attenuation model which has a T_{50} of 98 000 years (dividing 98 000 by 1.1 gets 89 000 which is approximately the T_{50} of the base model). The breakthrough times reflect the advective nature of benzene transport, as it takes about the same amount of time for groundwater to flow from the reservoir of interest to the spring. The attenuation model with $\lambda = 1.0^{-5}$ year^{-1} has the lowest concentration breakthrough at about 0.03 ppm; the model representing reservoir B has the highest breakthrough concentration. Clearly, both the distance to oil reservoir and the rate of biodegradation control the breakthrough concentration at the spring.

Diffusion versus advection

Prior studies use diffusion models to represent soluble benzene transport from oil deposits (Burtell & Jones 1996). Such decision is probably based on the observed exponential decrease of benzene concentration versus distance from the oil field. An exponential concentration/distance profile is characteristic of a diffusion-dominated system (Carslaw & Jaeger 1959). However, it can also characterize an advection dominated system modified by attenuation. To further evaluate the effect of diffusion versus advection, additional analytical analysis and numerical simulations are conducted.

For one-dimensional, non-reactive benzene diffusion through a homogenous and isotropic porous medium, the analytical solution of the diffusion equation is given as (Freeze & Cherry 1979):

$$\frac{C(x,t)}{C_0} = \mathrm{erfc}\left(\frac{x}{2\sqrt{Dt}}\right) \qquad (15)$$

where $C(x, t)$ is the concentration at distance x from the source at time t, C_0 is the constant solute concentration at

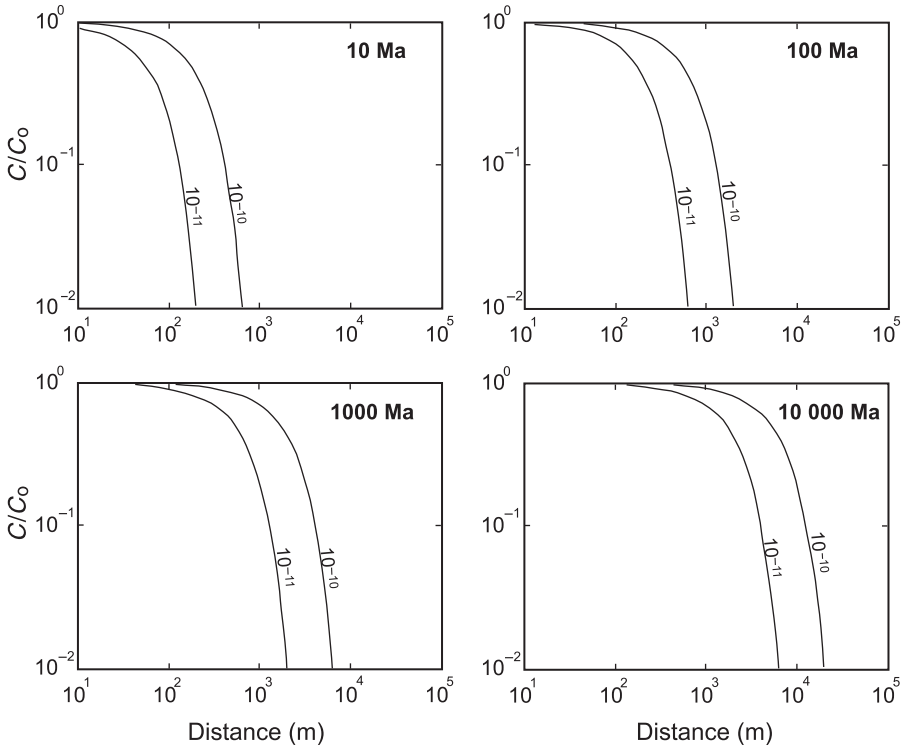

Fig. 14. One-dimensional analytical solution of the benzene diffusive front away from a source with a constant concentration (C_0) at 10, 100, 1000, and 10 000 Ma. Two diffusion coefficients (10^{-10} and 10^{-11} m^2 sec^{-1}) are used corresponding to the range measured in natural geological materials.

the source ($C(0, t) = C_0$ for all t), D is an effective diffusion coefficient. This solution assumes an initial concentration of 0.0 ppm within the solution domain at $x > 0.0$. Using representative effective diffusion coefficients ranging from 10^{-11} to 10^{-10} m^2 sec^{-1}, the diffusive solute front is calculated for different times (Fig. 14). The analytical results suggest that it would take approximately 100 Ma for benzene to diffuse 1 km and 1000 Ma to diffuse 4 km. To account for the observed maximum distance of 20 km, it would require a time span greater than 10 000 Ma which is older than the age of the Earth! Clearly, diffusion cannot account for the distances where elevated benzene concentration has been observed in Paleozoic formation waters adjacent to oil fields.

An idealized two-dimensional model domain is further developed to represent benzene diffusion, advection, and attenuation through a carrier bed adjacent to an oil reservoir (Fig. 15). The carrier bed is rectangular with a length of 10 km and a thickness of 400 m; the reservoir is located at the top left corner of the carrier bed with a length of 400 m and a thickness of 100 m. Due to this configuration, benzene transport is largely one-dimensional. This model is developed in an attempt to reproduce the measured benzene concentration reported from a number of oil fields across North America (Table 1). A permeability of 10^{-16} m^2 and porosity of 0.1 are assigned uniformly to both the carrier bed and the reservoir. For the advection model, a lateral head gradient of 0.015 is imposed on the carrier bed, resulting in a uniform flow field with an average groundwater velocity of 0.005 m year^{-1}. For the diffusion model, the same model domain is used with a head

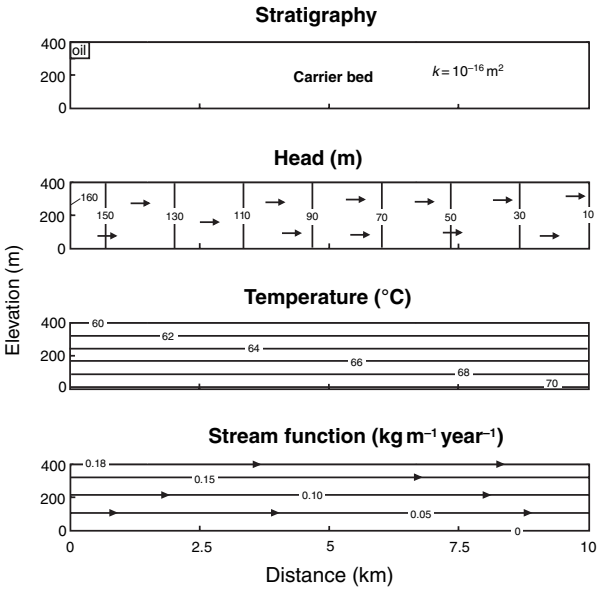

Fig. 15. Model domain for benzene transport within a carrier bed adjacent to an oil reservoir. The steady-state head, temperature, and stream function are computed for the advection model.

gradient set to zero across the carrier bed. Consequently, benzene diffusion dominates within the carrier bed. After 100 Ma, the diffusive benzene front has moved about 1 km from the reservoir, consistent with the prediction of the one-dimensional diffusion model (Fig. 14), but far from matching the field data (Fig. 16).

As diffusion alone cannot explain the observed field data within a reasonable geological time scale, we next consider whether advection/dispersion combined with biodegradation presents a more plausible mechanism. Different biodegradation rate constants (λ) are assigned to the advection/dispersion model which is run for up to 5 Ma. After 1 Ma, the advective/dispersive benzene front travels 6 km from the oil reservoir for the model with no biodegradation ($\lambda = 0$); 5 km for the model with $\lambda = 10^{-7}$ (not shown) and $\lambda = 10^{-6}$ year^{-1}, and 3 km for the model with $\lambda = 10^{-5}$ year^{-1} (Fig. 17A). For the given model temperature range (60–70°C; Fig. 15), the lower bound of the biodegradation rate constant chosen in the transport model ($\lambda = 10^{-6}$–10^{-7} year^{-1}) corresponds to the values estimated by Head *et al.* (2003). As the biodegradation rate increases, the distance benzene travels down gradient from the oil reservoir decreases. The benzene concentration is further sampled along a horizon within the carrier bed at 1, 2 and 5 Ma (Fig. 17B). The diffusion profile at 100 Ma and the field data from Zarrella *et al.* (1967) are also plotted. Given the different biodegradation rate constant assigned, the resulting advective/dispersive profiles encompass the field data after a few million years of transport. Also note the response of the concentration profile when the biodegradation rate is increased: when $\lambda = 10^{-7}$ year^{-1}, the profile is close to that of the no-biodegradation model and the benzene plume is moving away from the oil reservoir over time; when $\lambda = 10^{-5}$ year^{-1}, benzene plume in the carrier bed reaches a quasi-steady-state condition before 1 Ma, suggesting that attenuation within the carrier bed is vigorous enough to deter the advective/dispersive front from moving further. Exponential decrease of the concentration versus the distance from the oil reservoir is apparent in the advection/dispersion model with biodegradation. However, it is important to note that the biodegradation rate constants used by the advection model do not provide a unique fit to the field data. Several combinations of groundwater flow rates and biodegradation rate constants could account for the measured data.

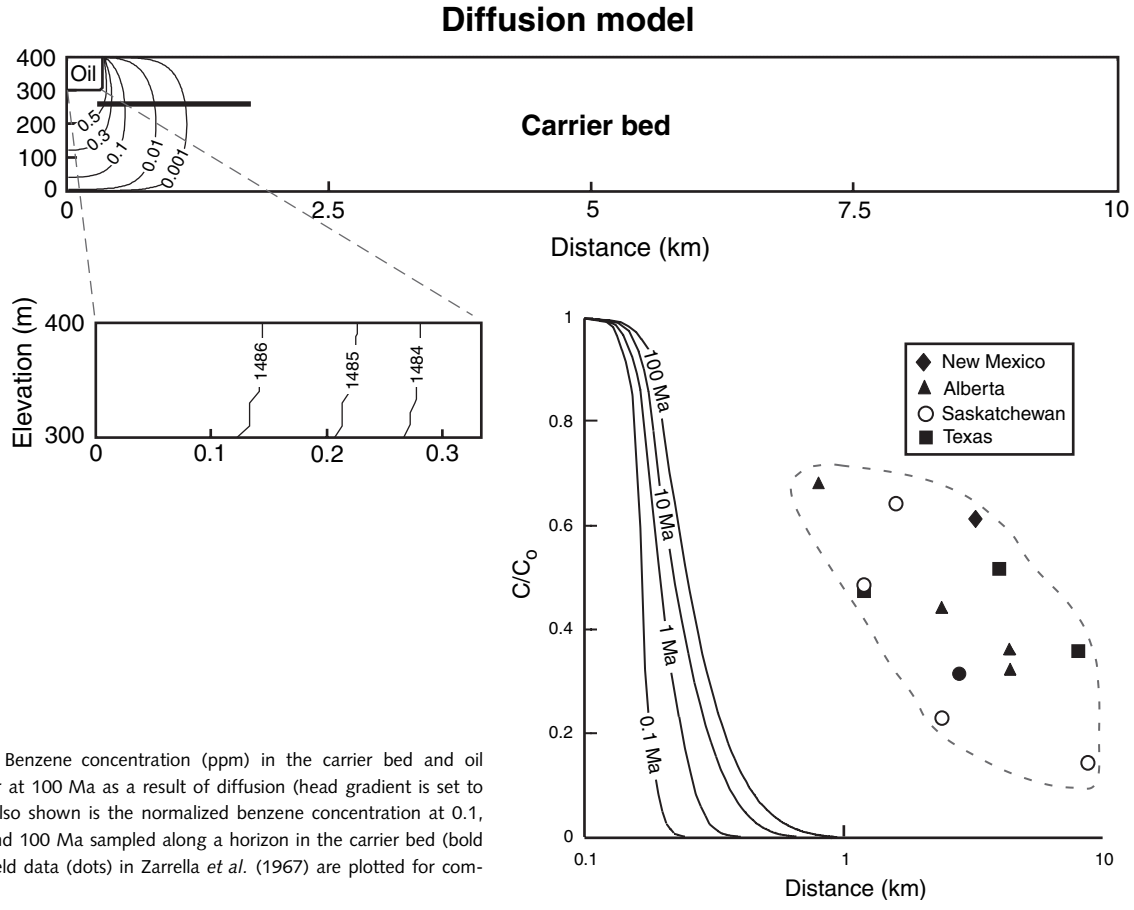

Fig. 16. Benzene concentration (ppm) in the carrier bed and oil reservoir at 100 Ma as a result of diffusion (head gradient is set to zero). Also shown is the normalized benzene concentration at 0.1, 1, 10 and 100 Ma sampled along a horizon in the carrier bed (bold line). Field data (dots) in Zarrella *et al.* (1967) are plotted for comparison.

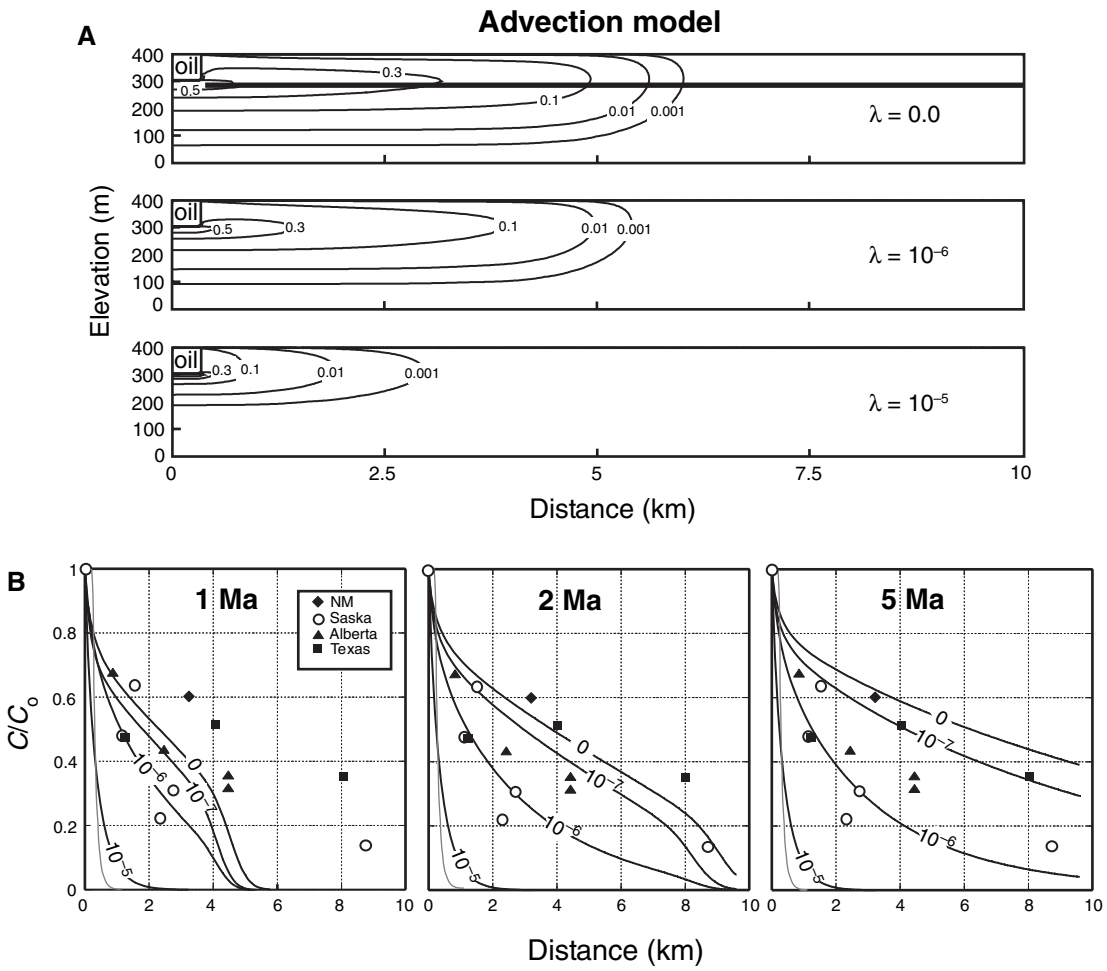

Fig. 17. (A) Benzene concentration (ppm) in the carrier bed at 1 Ma computed with the advection model. Various biodegradation rate constants are assigned ($\lambda = 0.0$, $\lambda = 10^{-6}$,$\lambda = 10^{-5}$ year^{-1}). (B) Benzene concentration sampled along a horizon within the carrier bed (bold line in A) at 1, 2, 5 Ma for various biodegradation rate constant ($\lambda = 0.0$, $\lambda = 10^{-7}$, $\lambda = 10^{-6}$, $\lambda = 10^{-5}$ year^{-1}). Field data (Zarrella *et al.* 1967) and the diffusive profile at 100 Ma (gray lines) are plotted for comparison.

DISCUSSION

The sensitivity study indicates that cap rock permeability can greatly affect the direction of soluble benzene migration and the location of its surface discharge in a basin. Given a favorable water table gradient that can induce upward groundwater flow within a cap rock, a potential exists for forming hydrodynamic surface anomalies adjacent to an oil field. In the sensitivity study, using an idealized basin with a cap rock permeability of 10^{-19} m^2, the computed upward groundwater velocity (v_z) within the cap rock above reservoir A is on the order of 10^{-6} m year^{-1}. Benzene diffusion dominates within the cap rock and the diffusive seepage will reach the water table after 5–6 Ma. Within the aquifer, benzene transport is dominated by advection and discharges at the spring. When the cap rock permeability is 10^{-17} m^2, it becomes sufficiently permeable (v_z is on the order of 10^{-4} m year^{-1}) to allow significant benzene advection towards the surface, forming a geochemical plume in the cap rock above the oil reservoir. After 1 Ma, surface benzene anomaly appears over a laterally extensive area adjacent to the oil field. A smaller anomaly also forms at the spring in one tenth of that time due to faster advection within the aquifer. When the cap rock permeability is 10^{-15} m^2 (v_z ranges from 10^{-3} to 10^{-2} m year^{-1}), local groundwater flow cells develop in the upper basin. Benzene is advected towards the surface and is not able to reach the spring. In this case, surface benzene anomaly appears in less than 0.1 Ma. Despite the variation in time that takes the surface anomalies to appear after the onset of reservoir flushing, once an oil reservoir is in place, benzene transport by groundwater can form surface anomalies nearly 'instantaneously' on a geologic time scale. However, significant upward benzene migration would not occur in the cap rock if the regional groundwater is flowing downwards above the oil reservoir (e.g. reser-

voir B). A possible exception would be if the cap rock permeability is less than 10^{-19} m^2 and upward diffusion within the cap rock would again dominate despite the unfavorable water table gradient.

The location of the surface benzene anomalies also varies depending on the direction of the groundwater flow within the cap rock. If groundwater flows vertically towards the surface, the peak benzene concentration may occur on the edge of the oil reservoir. If the groundwater flow is subvertical, the location of the peak surface concentration would shift towards the downstream direction. In both cases, positive temperature anomalies would form in the subsurface above the oil reservoir. If groundwater in the cap rock moves laterally or downwards, no edge effect can form in the vicinity of the oil field. In this case, negative temperature anomalies may form above the oil reservoir. In the sensitivity study, the various simulated locations and patterns of surface benzene anomalies can help explain why BTEX sometimes have been reported in regional groundwater discharge areas, not overlying any known oil deposits (Holysh & Tóth 1996); while other times they have been found in soils in vicinity of oil fields (e.g. Calhoun & Hawkins 1999).

For all the simulations conducted in this study, diffusion of benzene within the oil reservoir is found to be the rate-limiting factor for the coupled benzene mass transport process in the oil/water system. Tens of millions of years are required to flush benzene out of the oil reservoirs having thickness commensurate with those represented in this study, while it takes a fraction of that time for the dissolved benzene to reach the surface via advection. Moreover, lateral diffusion in groundwater cannot explain the observed distances dissolved benzene is found in formation waters adjacent to oil fields. Data by Zarrella *et al.* (1967) can best be explained by invoking an advection/dispersion model in which attenuation is also represented. The latter model can produce benzene concentration profiles that fall within the range of the field data after a few million years of transport. To reach the observed transport distances, a diffusion model would require a time span in excess of 1000 Ma. Since the benzene data from Zarrella *et al.* (1967) are mainly from Paleozoic or younger basins, the diffusion model appears unlikely.

Both the groundwater flow rate and the rate of biodegradation determine the distance of benzene transport from an oil reservoir. Depending on the flow rate, an increase of biodegradation rate by one order of magnitude can result in a decrease in the transport distance ranging from 3 to 30 km. The concentration at the spring is most sensitive to (i) distance from the upstream oil reservoir; (ii) rate of biodegradation. If dissolved benzene is found in springs, the upstream oil reservoir may lie within 20 km (the observed maximum transport distance) from the spring. Geochemical sampling of BTEX in springs can be a useful exploration tool only when the groundwater flow rate, direction as well as the BTEX biodegradation rate can be ascertained.

Finally, are there other possible explanations for the surface BTEX anomalies observed in the field, besides hydrodynamic transport by groundwater modeled in this study? For example, surface oil seeps are known to exist in many basins around the world (North 1985) and are used to locate some of the earliest discovered oil fields. It is possible that BTEX, as relatively light components of crude oil, can migrate with oil through fault or fracture networks which extend to the surface from the reservoir. To evaluate the relative efficiency of separate phase BTEX migration, a scale analysis is performed where separate phase oil migration is assumed to be driven by the density difference between the oil and formation water, and is assumed to occur along a fracture with an aperture width of 'b' (Fig. 18A). During the upward migration, BTEX is assumed to diffuse laterally out of the fracture into the surrounding formation water where initially no BTEX exist. The capillary force from the fracture wall is considered negligible and a constant diffusion coefficient of 10^{-11} m^2 sec^{-1} is assumed at all depth. By relating the time it would require for BTEX to diffuse out of the oil to the time it would take for the oil to reach the surface, the critical fracture aperture size can be computed which allows BTEX to reach the surface before completely diffusing out of the fracture (Fig. 18B). Using different crude oil densities and viscosities, we found that this critical aperture size is not sensitive to the depth of the oil reservoir, but is sensitive to oil types. The general range of the critical aperture estimated from this analysis is from 1.0 to 20.0 mm. The heavier the oil is, the wider the aperture it is required for BTEX to reach the surface. However, a fracture aperture much larger than 1.0 mm seems unrealistic. If a 10^8 bbl oil reservoir is connected to the land surface by a 1.0 mm fracture with a length of 1 km, it would only take an estimated 10^4 years to drain the entire reservoir by separate phase migration. Thus it appears unlikely that BTEX migrate with oil towards the surface and subsequently form geochemical anomalies. On the other hand, if BTEX are found in oil seeps, it might indicate a recent opening of a migration pathway.

One other possibility for BTEX migration towards the surface is through dissolution transport in gases. As temperature and pressure increase, crude oil solubility in light hydrocarbon gases such as methane increases (Price *et al.* 1983). BTEX, if dissolved in methane, could be brought towards the surface rapidly along fracture networks in the process of degassing. As the gaseous solution migrates upward, temperature and pressure decrease, the dissolved heavier hydrocarbons will experience retrograde condensation. BTEX may then exsolve to form liquids and be subject to either buoyancy transport or miscible transport by groundwater. These complex and possibly concurrent processes need to be studied in a quantitative manner if we

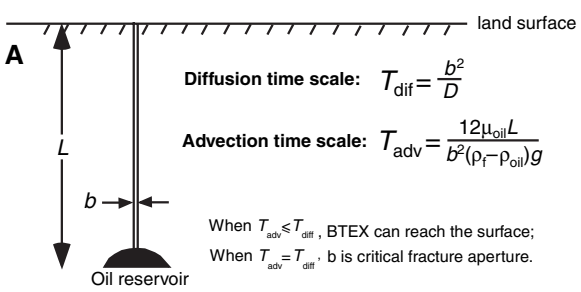

B

Oil Name	API	Density (g ml^{-1})	Viscosity (Pa·s)	Symbol
California (API 11)	10.3	0.988	34	
Asphalt primer	18.6	0.94	3.28	
Alaska north slope	26.8	0.90	0.023	
Arabian heavy	27.4	0.89	0.041	
Arabian light	32.5	0.86	0.014	
Avalon	36	0.844	0.011	
Alberta	36.8	0.84	0.006	
Aviation gasoline 80	71.8	0.69	0.001	

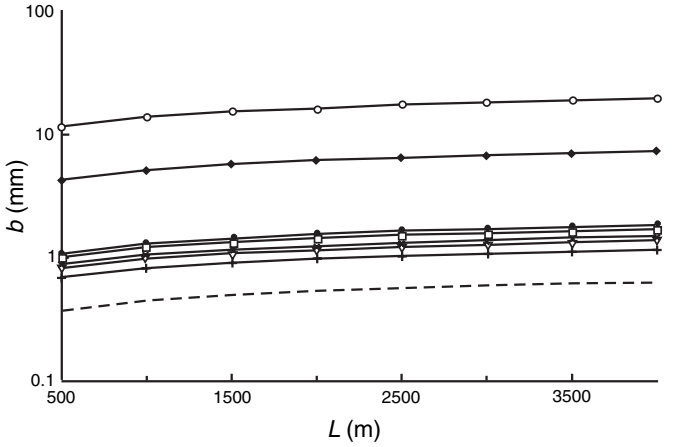

Fig. 18. (A) A schematic diagram showing an oil reservoir at depth L which is connected to the land surface via a fracture with an aperture size of b. T_{dif} is the time required for benzene to diffuse a distance of b; T_{adv} is the time required for oil to reach the surface via buoyancy. (B) The critical fracture aperture size b (mm) calculated for different oil density and viscosity at 15 ± 3°C (Oil Properties database, Environmental Technology Center, Canada; http://www.etcentre.org).

are to fully understand the perplexing arrays of surface and subsurface hydrocarbon anomalies. In addition, lighter C_2–C_5 hydrocarbons such as ethane, propane, butane and pentane are also water-soluble with solubilities increasing with depth (McAuliffe 1963; Carroll & Mather 1997). They are also biodegradable (Head *et al.* 2003). However, upon finding BTEX or the lighter hydrocarbons at the surface, we shall refrain from drawing an immediate conclusion that any particular transport mechanism has occurred. Careful investigation including the identification of potential fracture networks and the evaluation of the hydrological and thermal conditions of the field is necessary to determine the dominant transport mechanism(s).

In summary, aqueous transport of BTEX in groundwater and the associated surface and subsurface geochemical anomalies are influenced by the variations in the cap rock permeability, the location of the oil reservoir in relation to the regional groundwater flow field, and the subsurface biodegradation conditions. Convective subsurface temperature anomalies can also form in association with the geochemical anomalies and can indicate the direction of groundwater flow. Unless extensive fracture networks exist between the oil reservoir and the land surface, BTEX soil gas anomalies are likely controlled by regional hydrodynamics rather than separate phase migration. To conduct oil exploration using BTEX as geochemical indicators, the subsurface hydrological, thermal and geochemical conditions have to be evaluated carefully, along with the examination of the presence/absence of any fracture networks. Knowledge of the regional groundwater flow system as well as the general range of the cap rock permeability should help in the better interpretation of the BTEX surface and subsurface anomalies. This is in agreement with Tóth (1996).

CONCLUSIONS

In this study, a suite of numerical experiments is conducted to gain insight into the aqueous transport and attenuation of petroleum-derived benzene in sedimentary basins. Using an idealized basin cross-section, benzene transport in the basin is represented by advective/dispersive solute transport in groundwater along with bacterial attenuation. Benzene transport within the oil reservoir is represented by a diffusion model. Mass transfer at the oil–water contact is described using a first-order Newtonian mass transfer law assuming equilibrium partitioning. A sensitivity study is conducted to evaluate the influence of the variations of the hydrologic and geochemical parameters on soluble benzene migration in basins. The oil reservoir location is also varied in relation to the regional groundwater discharge area.

Results of the sensitivity study indicate that in basins with active hydrodynamics (i.e. groundwater flow rate $>10^{-6}$ m year^{-1}), benzene transport is dominated by advection. If dissolved benzene is found in dry wells intersecting an active flow field, the unknown oil reservoir is most likely located hydraulically up-gradient. The diffusion model requires unrealistic time scales to permit kilometer-scale migration, while diffusion may dominate within the cap rock when its permeability is less than 10^{-19} m^2. Transport of benzene by groundwater can also form surface geochemical anomalies, sometimes adjacent to the oil fields. Distance of benzene transport away from the oil

reservoir is determined by the groundwater velocity and the biodegradation rate constant. Vertical migration of BTEX as gas bubbles from oil reservoirs does not appear likely. Excluding contamination from fuel spills, soil BTEX gas anomalies are likely the result of volatization at the water table during the final stage of their migration, either as separate phase flow or as dissolved solutes in groundwater/gases. In the case of buoyancy-driven separate phase migration, a fracture aperture size of 1.0 mm or larger may be required for BTEX to reach the surface. Surface geochemical exploration based on BTEX soil gas anomalies can be effective only after the various transport mechanism(s) is understood and their migration pathway(s) delineated. It's important to point out that shallow groundwater and soils near many existing oil fields have been contaminated with BTEX (Blake 2000). Surface geochemical explorations near known fields have to exercise caution to exclude such possibilities.

Future research should be directed towards field sampling of wells down gradient from known oil fields in conjunction with mathematical modeling. Laboratory column experiments should be conducted under reservoir temperature/pressure conditions using microbes extracted from strata near oil reservoirs to estimate the *in-situ* BTEX biodegradation rate. Studies of BTEX migration in oil-bearing marine basins would shed light on their transport in the relatively low velocity environment. Dissolution transport of the C2–C5 hydrocarbons by groundwater in contact with oil or gas reservoirs should also be quantitatively evaluated.

ACKNOWLEDGEMENTS

The study reported here was funded by the US Department of Energy, National Petroleum Technology Office (NPTO) in Tulsa, Oklahoma (Project ID: P/INEEL-DPR5A404). We acknowledge the sincere assistance of the computing support staff: Peng Wang and Mary Papakhian at UITS of the Indiana University. We thank Prof. H.C. Helgeson, University of California, at Berkeley, for providing us with SUPCRT92. We greatly appreciate our reviewers' comments and suggestion, and have added a discussion on 'salting-out' effect as well as updated some of our biodegradation discussions.

REFERENCES

Aljoe KJ, Ferguson AM, Bailey D, Gadalla N, Boyd B, Rodgers AS, Chao J, Somayajulu GR, Das A (1986) *TRC Thermodynamic Tables, Hydrocarbons.* Texas A&M University. Thermodynamics Research Center, National Institute of Standards and Technology http://trc.nist.gov/tables/hydro.htm.

Appold MS, Garven G (1999) The hydrology of ore formation in the southeast Missouri district: numerical models of topography-driven fluid flow during the Ouachita orogeny. *Economic Geology*, **94**, 913–36.

Allen-King RM, O'Leary KE, Gilham RW, Barker JF (1994) Limitations on the biodegradation rate of dissolved BTEX in a natural, unsaturated, sandy soil; evidence from field and laboratory experiments. *Bioremediation*, **2**, 175–91.

Allin DL (1990) Colorado plateau subsurface water flow key. *Oil and Gas Journal*, **July 23**, 52–4.

Atlas RM (1984) *Petroleum Microbiology.* Macmillan Company, New York.

Banerjee S (1984) Solubility of organic mixtures in water. *Environmental Science and Technology*, **18**, 587–91.

Barbaro JR, Barker JF, Lemon LA, Mayfield CI (1992) Biotransformation of BTEX under anaerobic, denitrifying conditions: field and laboratory observations. *Journal of Contaminant Hydrology*, **11**, 245–72.

Barker JF, Patrick GC, Major D (1987) Natural attenuation of aromatic hydrocarbons in a shallow sand aquifer. *Ground Water Monitoring Review*, **7**, 64–71.

Barker JF, Patrick GC, Berwanger DJ, Sudicky EA (1989) Leaky microcosms are representative of BTX biodegradation in the Borden sand aquifer. In: *Proceedings of the Conference on New Field Techniques for Quantifying the Physical and Chemical Properties of Heterogeneous Aquifers*, pp. 795–814. National Water Well Association, Dublin, OH.

Bear J (1988) *Dynamics of Fluids in Porous Media.* Dover Publications, New York.

Blake K (2000) Trees suck … BTEX compounds from shallow soils and groundwater. *AAPG Bulletin*, **84**, 859.

Borden RC, Daniel RA, LeBrun LE, Davis CW (1997a) Intrinsic biodegradation of MTBE and BTEX in a gasoline-contaminated aquifer. *Water Resources Research*, **33**, 1105–15.

Borden RC, Goin RT, Kao CM (1997b) Control of BTEX migration using a biologically enhanced permeable barrier. *Ground Water Monitoring and Remediation*, **17**, 70–80.

Bredehoeft JD, Bennett RR (1972) Potentiometric surface of the Tensleep sandstone in the Big Horn basin, west-central Wyoming, 1:250,000. *USGS open-file Map No. 72-461.*

Burland SM, Edwards EA (1999) Anaerobic benzene biodegradation linked to nitrate reduction. *Applied and Environmental Microbiology*, **65**, 529–33.

Burtell SG, Jones VT (1996) Benzene content of subsurface brines can indicate proximity of oil, gas. *Oil and Gas Journal*, **94**(3), 59–64.

Calhoun GG, Hawkins JL (1998) BTEX detector's results good in oil identification. *Oil and Gas Journal*, **30**, 77–80.

Calhoun GG, Hawkins JL (1999) BTEX geochemical investigation, Permian Basin. In: *AAPG Annual Meeting Expanded Abstracts*, P. A19. San Antanio, Texas, April 11–14.

Carroll JJ, Mather AE (1997) A model for the solubility of light hydrocarbons in water and aqueous solutions of alkanolamines. *Chemical Engineering Science*, **52**, 545–52.

Carslaw HS, Jaeger JC (1959) *Conduction of Heat in Solids.* Oxford University Press, New York.

Chapelle FH, Bradley PM, McMahon PB (1993) Subsurface microbiology. In: *Regional Groundwater Quality*, pp. 181–98. Van Nostrand Reinhold, New York.

Chrysikopoulos CV, Lee KY (1998) Contaminant transport resulting from multicomponent nonaqueous phase liquid pool dissolution in three-dimensional subsurface formations. *Journal of Contaminant Hydrology*, **31**, 1–21.

Freeze RA, Cherry JA (1979) *Groundwater.* Prentice-Hall, Englewood Cliffs, NJ.

Garven G (1989) A hydrogeologic model for the formation of the giant oil sands deposits of the Western Canada sedimentary basin. *American Journal of Science*, **289**, 105–66.

Garven G, Freeze RA (1984) Theoretical analysis of the role of groundwater flow in the genesis of stratabound ore deposits; 1, Mathematical and numerical model. *American Journal of Science*, **284**, 1085–124.

Gillham RW, Burris DR (1992) Recent developments in permeable in situ treatment wells for remediation of contaminated groundwater. In: *Proceedings, Subsurface Restoration Conference, June 21–24, 1992*, Dallas, Texas.

Hanshaw BB, Hill GA (1969) Geochemistry and hydrodynamics of the Paradox Basin region, Utah, Colorado, and New Mexico. *Chemical Geology*, **4**, 263–94.

Hawkins JL, Calhoun GG (2001) Groundwater seems not to influence BTEX subface geochemistry. *Oil and Gas Journal*, **99**(41), 32–6.

Head IM, Jones DM, Larter SR (2003) Biological activity in the deep subsurface and the origin of heavy oil. *Nature*, **426**, 344–52.

Helgeson HC (1969) Thermodynamics of hydrothermal systems at elevated temperatures and pressures. *American Journal of Science*, **267**, 729–804.

Helgeson HC, Owens CE, Knox AM, Richard L (1998) Calculation of the standard molal thermodynamic properties of crystalline, liquid, and gas organic molecules at high temperatures and pressures. *Geochimica et Cosmochimica Acta*, **62**, 985–1081.

Holysh S, Tóth J (1996) Flow of formation waters: likely cause for poor definition of soil gas anomalies over oil fields in east-central Alberta, Canada. *AAPG Memoir*, **66**, 255–77.

Huang H, Larter SR, Bowler BFJ, Oldenburg TBP (2004) A dynamic biodegradation model suggested by petroleum compositional gradients within reservoir columns from the Liaohe basin, NE China. *Organic Geochemistry*, **35**, 299–316.

Hubbert MK (1953) Entrapment of petroleum under hydrodynamic conditions. *AAPG Bulletin*, **37**, 1954–2026.

Hunt JM (1979) *Petroleum Geochemistry and Geology*, pp. 448–50. W H Freeman & Col, San Francisco, CA.

IUPAC Solubility Data Series (1989) *Hydrocarbons with Water and Seawater*. Pergamon Press, New York.

Jamison VW, Raymond RL, Hudson JO (1976) Biodegradation of high-octane gasoline. In: *Proceedings of the Third International Biodegradation Symposium*, pp. 187–96. Applied Science, London.

Johnson JW, Oelkers EH, Helgeson HC (1992) SUPCRT92: A software package for calculating the standard molal thermodynamic properties of minerals, gases, aqueous species, and reaction from 1 to 5000 bar and 0 to 1000°C. *Computers and Geosciences*, **18**, 899–947.

Jones VT (1984) *Overview of Geochemical Exploration Technology, a Short Course on Geochemical Exploration Technology*. Rocky Mountain Association of Geologists, Denver.

Jury WA, Gardner WR, Gardner WH (1991) *Soil Physics*, 5th edn. John Wiley & Sons, New York.

Kazumi J, Caldwell ME, Suflita JM, Lovely DR, Young LY (1997) Anaerobic degradation of benzene in diverse anoxic environments. *Environmental Science and Technology*, **31**, 813–8.

Kestin J, Khalifa HE, Corriea R (1981) Tables of the dynamics and kinematic viscosity of aqueous NaCl solutions in the temperature range of 20–50°C and the pressure range of 0.1–35 Mpa. *Journal of Physical Chemistry Reference Data*, **10**, 71–87.

Kuo LC (1994) An experimental study of crude oil alteration in reservoir rocks by water washing. *Organic Geochemistry*, **21**, 465–79.

Lafargue E, Thiez PL (1996) Effect of waterwashing on light ends compositional heterogeneity. *Organic Geochemistry*, **24**, 1141–50.

Landmeyer JE, Chapelle FH, Petkewich MD, Bradley PM (1998) Assessment of natural attenuation of aromatic hydrocarbons in groundwater near a former manufactured-gas plant, South Carolina, USA. *Environmental Geology*, **34**, 279–92.

Larter SR, Bennett B, Chen M, Bowler BFJ, Dale JD, Aplin AC (1997) Interaction of polar compounds between oil, water and rock; towards a new generation of reservoir geochemical tools. In: *AAPG Annual Meeting Abstracts*, pp. 66–7.

Lipson D, Siegel DI (2000) Using ternary diagrams to characterize transport and attenuation of BTX. *Ground Water*, **38**, 106–13.

Lu G, Clement TP, Zheng C, Wiedemeier TH (1999) Natural attenuation of BTEX compounds: model development and field-scale application. *Ground Water*, **37**, 707–17.

Ma Y, Kemblowski MW, Urroz GE (1999) A Heuristic model of aerobic biodegradation of dissolved hydrocarbons in aquifers. *Ground Water*, **37**, 491–7.

Machel HG, Burton EA (1991) Causes and spatial distribution of anomalous magnetization in hydrocarbon seepage environments. *AAPG Bulletin*, **75**, 1864–76.

McAuliffe C (1963) Solubility in water of C1–C9 hydrocarbons. *Nature*, **200**, 1092–3.

North FK (1985) *Petroleum Geology*. Allen & Unwin, London.

O'Leary KE, Barker JF, Gilham RW (1995) Remediation of dissolved BTEX through surface application: a prototype field investigation. *Ground Water Monitoring and Remediation*, **15**, 99–109.

Odermatt JR (1994) Natural chromatographic separation of benzene, toluene, ethylbenzene and xylenes (BTEX compounds) in a gasoline contaminated ground water aquifer. *Organic Geochemistry*, **21**, 1141–50.

Parker JC (1989) Multiphase flow and transport in porous media. *Reviews of Geophysics*, **27**, 311–28.

Patrick GC, Barker JF (1985) A natural-gradient tracer study of dissolved benzene, toluene and xylenes in ground water. In: *Second Canadian/American Conference on Hydrogeology; Hazardous Wastes in Ground Water; a Soluble Dilemma*, pp. 141–7. National Water Well Association, Dublin, OH.

Philp RP, Crisp PT (1982) Surface geochemical methods used for oil and gas prospecting, a Review. *Journal of Geochemical Exploration*, **17**, 1–34.

Powers S, Loureiro CO, Abriola LM, Weber WJ (1991) Theoretical study of the significance of nonequilibrium dissolution of nonaqueous phases in subsurface systems. *Water Resources Research*, **27**, 463–77.

Prausnitz JM, Lichtenthaler RN, de Azevedo EG (1999) *Molecular Thermodynamics of Fluid-Phase Equilibria*, 3rd edn. Prentice-Hall PTR, Upper Saddle River, NJ.

Price LC (1985) A critical overview of and proposed working model for hydrocarbon microseepage. *USGS Open-File Report*, pp. 85–271.

Price LC, Wenger LM, Ging T, Blount CW (1983) Solubility of crude oil in methane as a function of pressure and temperature. *Organic Geochemistry*, **4**, 201–21.

Reid RC, Prausnitz JM, Poling BE (1987) *The Properties of Gases and Liquids*, 4th edn. McGraw-Hill, New York.

Richard L, Helgeson HC (1998) Calculation of the thermodynamic properties at elevated temperatures and pressures of saturated and aromatic high molecular weight solid and liquid hydrocarbons in kerogen, bitumen, petroleum, and other organic matter of biogeochemical interest. *Geochimica et Cosmochimica Acta*, **62**, 3591–636.

Rostron BJ, Tóth J (1996) Ascending fluid plumes above Devonian pinnacle reefs: numerical modeling and field examples from west-central Alberta, Canada. *AAPG Memoir*, **66**, 185–201.

Saunders DF, Burson KR, Thompson CK (1999) Model for hydrocarbon microseepage and related near-surface alterations. *AAPG Bulletin*, **83**, 170–85.

Schirmer M, Butler BJ, Barker JF, Church CD, Schirmer K (1999) Evaluation of biodegradation and dispersion as natural

attenuation processes of MTBE and benzene at the Borden field site. *Physical, Chemical and Earth Sciences*, **24**, 557–60.
Schumacher D (1999) Surface geochemical exploration for petroleum. In: *Exploring for Oil and Gas Traps*. AAPG, Tulsa, OK.
Schwille F (1981) Groundwater pollution in porous media by fluids immiscible with water. In: *Quality of Groundwater, Proceedings of an International Symposium*. (eds van Duijvenbooden W, Glosbergen P, van Lelyveld H). Elsevier, Amsterdam.
Shock EL, Helgeson HC (1990) Calculation of the thermodynamic and transport properties of aqueous species and high pressures and temperatures: Standard partial molal properties of organic species. *Geochimica et Cosmochimica Acta*, **54**, 915–45.
Suarez MP, Rifai HS (2004) Modeling natural attenuation of total BTEX and benzene plumes with different kinetics. *Ground Water Monitoring and Remediation*, **24**, 53–68.
Sudicky EA, MacQuarrie K (1989) Behaviour of biodegradable organic contaminants in random stationary hydraulic conductivity fields. In: *Contaminant Transport in Groundwater, Proceedings of an International Symposium*. (eds Kobus HE & Kinzelbach W). A.A Balkema Rotterdam-Brookfield, International, Rotterdam.
Tóth J (1963) A theoretical analysis of groundwater flow in small drainage basins. *Journal of Geophysical Research*, **68**, 4795–812.
Tóth J (1996) Thoughts of a hydrogeologist on vertical migration and near-surface geochemical exploration for petroleum. *AAPG Memoir*, **66**, 279–83.
Walvoord MA, Pegram P, Phillips FM, Person M, Kieft TL, Fredrickson JK, McKinley JP, Swenson JB (1999) Groundwater flow and geochemistry in the southeastern San Juan Basin: implications for microbial transport and activity. *Water Resources Research*, **35**, 1409–24.
Weiner JM, Lovley DR (1998a) Anaerobic benzene degradation in petroleum-contaminated aquifer sediments after inoculation with a benzene-oxidizing enrichment. *Applied and Environmental Microbiology*, **64**, 775–8.
Weiner JM, Lovley DR (1998b) Rapid benzene degradation in methanogenic sediments from a petroleum-contaminated aquifer. *Applied and Environmental Microbiology*, **64**, 1937–9.
Weisenburg DA, Bodennec G, Brooks JM (1981) Volatile liquid hydrocarbons around a productive platform in the northwest Gulf of Mexico. *Bulletin Environmental Contamination Toxicology*, **27**, 167–74.
Zarrella WM, Mousseau RJ, Coggeshall ND, Norris MS, Schrayer GJ (1967) Analysis and significance of hydrocarbons in subsurface brines. *Geochimica et Cosmochimica Acta*, **31**, 1155–66.
Zheng C, Bennett GD (1995) *Applied Contaminant Transport Modeling*. Van Nostrand Reinhold, New York.
Zhu C (2000) Estimate of recharge from radiocarbon dating of groundwater and numerical flow and transport modeling. *Water Resources Research*, **36**, 2607–20.

NOMENCLATURE

∇	Gradient operator
$\cdot$	Inner product
h	Hydraulic head
$\vec{q}$	Darcy flux: $\vec{q} = \begin{bmatrix} q_x \\ q_z \end{bmatrix}$
$\lvert\vec{q}\rvert$	Magnitude of the Darcy flux
ϕ	Porosity
$\vec{v}$	Groundwater velocity: $\vec{v} = \vec{q}/\phi$; $\vec{v} = \begin{bmatrix} v_x \\ v_z \end{bmatrix}$
$\lvert\vec{v}\rvert$	Magnitude of the groundwater velocity
ρ_f	Density of water
ρ_{oil}	Density of oil
ρ_r	Relative water density ($\rho_r = (\rho_f - \rho_0)/\rho_0$)
μ_r	Relative water viscosity ($\mu_r = \mu_0/\mu_f$)
μ_f	Dynamic water viscosity
μ_{oil}	Dynamic oil viscosity
ρ_0	Reference density of fresh water at 20°C and 1.01×10^5 Pa
μ_0	Reference viscosity of fresh water at 20°C and 1.01×10^5 Pa
$\mathbf{K}$	Hydraulic conductivity tensor: $\mathbf{K} = \begin{bmatrix} K_{xx} & K_{xz} \\ K_{zx} & K_{zz} \end{bmatrix}$
$\lvert\mathbf{K}\rvert$	Determinant of $\mathbf{K}$
K_{max}	Maximum principal conductivity
K_{min}	Minimum principal conductivity
θ	Dip angle of a hydrostratigraphic unit relative to horizontal plane
$\mathbf{k}$	Permeability tensor
Ψ	Mass-based stream function
T	Temperature of water
∇T	Temperature gradient
$\boldsymbol{\lambda}$	Thermal conduction–dispersion tensor: $\boldsymbol{\lambda} = \begin{bmatrix} \lambda_{xx} & \lambda_{xz} \\ \lambda_{zx} & \lambda_{zz} \end{bmatrix}$
c_f	Specific heat capacity of water
α_L	Longitudinal dispersivity
α_T	Transverse dispersivity
λ_f	Thermal conductivity of water
λ_s	Thermal conductivity of porous rocks
R	Retardation factor
C_w	Aqueous benzene concentration
λ	First-order biodegradation rate constant
$\mathbf{D}$	Hydrodynamic diffusion–dispersion tensor: $\mathbf{D} = \begin{bmatrix} D_{xx} & D_{xz} \\ D_{zx} & D_{zz} \end{bmatrix}$
D_{aq}^e	Effective benzene diffusion coefficient in aquifer
D_{oil}^e	Effective benzene diffusion coefficient in oil reservoir
C_{oil}	Benzene concentration in oil
S_w	Water saturation ratio
S_{oil}	Oil saturation ratio
D_{aq}	Benzene diffusion coefficient in water
D_{oil}	Benzene diffusion coefficient in oil
C_6H_6	Chemical formula for benzene
k_f	Mass transfer coefficient
C_I	Aqueous benzene concentration at the phase boundary
J	Benzene mass flux across the oil–water contact
Γ	Equilibrium partition coefficient (ppm/ppm)
Γ^*	Equilibrium partition coefficient (molality/mole fraction)
K	Equilibrium constant of the benzene dissolution reaction
a_{aq}	Activity of aqueous benzene
a_{oil}	Activity of oil-phase benzene
m_{aq}	Molality of aqueous benzene
X_{oil}	Mole fraction of oil-phase benzene
γ_{aq}	Activity coefficient of benzene in water
f_{oil}	Activity coefficient of benzene in oil
$m_{aq}^{solubility}$	Pure liquid solubility
S_h	Sherwood number (dimensionless)
R_e	Reynolds number (dimensionless)
S_c	Schmidt number (dimensionless)